The Generation and Compaction of Partially Molten Rock

by DAN McKENZIE

Bullard Laboratories of the Department of Earth Sciences, Madingley Rise, Madingley Road, Cambridge CB3 0EZ, U.K.

(*Received 9 September 1983; in revised form 16 March 1984*)

ABSTRACT

The equations governing the movement of the melt and the matrix of a partially molten material are obtained from the conservation of mass, momentum, and energy using expressions from the theory of mixtures. The equations define a length scale δ_c called the compaction length, which depends only on the material properties of the melt and matrix. A number of simple solutions to the equations show that, if the porosity is initially constant, matrix compaction only occurs within a distance $\sim\delta_c$ of an impermeable boundary. Elsewhere the gravitational forces are supported by the viscous stresses resulting from the movement of melt, and no compaction occurs. The velocity necessary to prevent compaction is known as the minimum fluidization velocity. In all cases the compaction rate is controlled by the properties of the matrix. These results can only be applied to geological problems if the values of the permeability, bulk and shear viscosity of the matrix can be estimated. All three depend on the microscopic geometry of the melt, which is in turn controlled by the dihedral angle. The likely equilibrium network provides some guidance in estimating the order of magnitude of these constants, but is no substitute for good measurements, which are yet to be carried out. Partial melting by release of pressure at constant entropy is then examined as a means of produced melt within the earth.

The principal results of geological interest are that a mean mantle temperature of 1350 °C is capable of producing the oceanic crustal thickness by partial melting. Local hot jets with temperatures of 1550 °C can produce aseismic ridges with crustal thicknesses of about 20 km on ridge axes, and can generate enough melt to produce the Hawaiian Ridge. Higher mantle temperatures in the Archaean can produce komatiites if these are the result of modest amounts of melting at depths of greater than 100 km, and not shallow melting of most of the rock. The compaction rate of the partially molten rock is likely to be rapid, and melt-saturated porosities in excess of perhaps 3 per cent are unlikely to persist anywhere over geological times. The movement of melt through a matrix does not transport major and trace elements with the mean velocity of the melt, but with a slower velocity whose magnitude depends on the distribution coefficient. This effect is particularly important when the melt fraction is small, and may both explain some geochemical observations and provide a means of investigating the compaction process within the earth.

INTRODUCTION

There is an obvious need for a simple physical model which can describe the generation of a partially molten rock, and the separation of the melt from the residual solid, which will be referred to as the matrix. If such a model is to be useful it must lead to differential equations which can be solved by standard methods. The principal aim of this paper is to propose such a model, derive the governing equations, and obtain some solutions for particularly simple cases. The model is concerned with the physics, rather than the chemistry, of the process, though the formulation is sufficiently general to allow the inclusion of complicated phase equilibria. Several effects whose importance is unclear have not been included, in order to obtain the simplest model which can describe the generation and extraction of magma.

Generation of a magma containing few solid crystals requires two operations. A partially molten rock must first be generated, either by supplying heat or by reducing the pressure and so changing the solidus temperature. Once such a rock has been formed, the melt must

separate from the residual solid matrix. Such separation is only possible if there is relative motion between the matrix and the melt, and therefore this process involves two phase flow. In practice these two processes are unlikely to be independent, since melt extraction will occur at the same time as melt is being generated.

There has been considerable interest for some time among geophysicists and petrologists in the dynamics of partially molten rocks. All of this work has been hindered by the difficulty of describing the fluid mechanical behaviour of the crystalline residue. Several authors (Walker *et al.*, 1978; Ahern & Turcotte, 1979; Maaløe & Scheie, 1982) have argued that the rate at which the matrix will compact will be governed only by the rate at which the melt can be expelled, and not by the mechanical properties of the matrix. The equations obtained below show that this argument is not correct, and that the expulsion rate always depends on the properties of the matrix. Some other authors have attempted to take account of matrix deformation. Sleep (1974) wrote down the equations governing conservation of mass and momentum for two phase flow, though he made little attempt to obtain solutions. He did not, however, include the bulk viscosity of the matrix. Stolper *et al.* (1981) attempted to take account of the matrix deformation without obtaining the general equations, but their results do not agree with those obtained below. Waff (1980) has argued that static solutions exist in which finite melt fractions are stationary with respect to the matrix. No such solutions are obtained here, and it is unlikely that they are stable. Maaløe & Scheie (1982) have proposed the form of the flow between melt and matrix, and have even attempted to investigate its stability. They also did not start from the conservation equations. Their problem is considerably more complicated than any of those examined below, and it remains to be seen whether their proposals are correct.

The approach taken below most closely resembles that of Sleep (1974), and starts from the general differential equations which govern two phase flow in a material which is melting (Appendix A). These equations govern the conservation of mass, momentum and energy in the material, and therefore provide the mathematical basis for all further investigations. They are, however, rather complicated, especially the energy equation, and experience in other areas of fluid dynamics shows that it is useless to attempt to solve such equations directly and to include every effect which is believed to be important geologically. The way to proceed is to solve a succession of simplified problems of gradually increasing complexity, using the understanding gained from the simpler problems to understand the behaviour of the more complicated ones. This process is familiar to igneous petrologists when it is applied to phase diagrams of coexisting minerals, but is is perhaps less obvious that this is the correct approach when the problems involve mathematial equations, especially when some of the simpler problems have limited geological interest.

Various model problems are examined below. The first simplification made is to separate the melting problem from that of compaction. This result is achieved by not allowing relative motion between the melt and matrix during melting, and then considering the compaction of a partially molten region as a separate problem. Since the equations governing compaction are new, the nature of their solutions must be investigated systematically. The first step in doing so is to obtain analytic solutions where possible. Several such solutions are obtained in Appendix B, and demonstrate that there are two types of flow in such regions. Boundary layers exist in which compaction of the matrix occurs. The interior flow consists of uniform movement of the melt without any associated compaction. These analytic solutions must form the basis of any investigation of the non-linear behaviour which occurs when appreciable compaction has taken place. Though the initial and boundary conditions of these analytic solutions are not those appropriate to, for instance, magma generation beneath ridge axes, it is essential to understand how simple systems behave before attempting to investigate

real geological problems. There would, for instance, be little point in studying the melting behaviour of a garnet peridotite in the laboratory if the existence of eutectics in two component systems was unknown.

The equation governing the conservation of energy is more complicated than those governing the conservation of mass and momentum. It contains terms which take account of the latent heat of melting, the transport of heat by the separate movement of the melt and the matrix, and the heat generated by the deformation of the melt and the matrix. Little is yet known about the solutions to this equation, so once again a number of simplified problems must first be considered. The two discussed here are melting at constant entropy produced by upwelling, with no motion between melt and matrix (Appendix D), and the distribution of heat generation by deformation of the melt and matrix (Appendix B). Melting at constant entropy is probably a reasonable approximation to the behaviour of the mantle beneath both ridge axes and intraplate volcanoes, though probably not beneath island arcs, and therefore an attempt is made to obtain empirical relationships between the temperature, pressure and melt fraction, and to carry out realistic calculations.

Modern geochemistry makes much use of trace element distributions, and it is of interest to examine how both major and trace elements move during two phase flow. The governing equation resembles that of energy conservation, and an analytic solution can be obtained to a simplified problem of melt moving through a matrix which is neither compacting nor melting (Appendix E).

A major advantage of approaching problems in the manner outlined above is that analogies between different problems can be exploited. For instance there are at least four problems of geological interest which are concerned with the fluid dynamics of two phase flow. One is the magma extraction problem. Another is the compaction of sediments during burial by the expulsion of water. This problem is better understood than that of magma extraction, because of its importance to the oil industry. Many of the effects which are investigated below using simplified model problems, such as fluidization, dispersion and differential transport of solutes, are well known in other contexts. Several other more complicated effects which are known to take place in compacting sediments, and which are less easily modelled, should also occur in partially molten rocks.

A third problem of geological interest which involves two phase flow is the movement of fluids, such as water and carbon dioxide, during crustal metamorphism (Elliot, 1973; Durney, 1976; Rutter, 1976). This problem is obviously similar to the igneous problem, but it is more difficult because the fluids involved cannot be directly sampled and the minerals of the matrix are often undergoing phase changes. Some useful results can nonetheless be obtained (Bickle & McKenzie, in preparation).

A further example of two phase flow is the growth of the inner core. The molten iron of which the outer core consists probably also contains a small proportion of a lighter element. The solid inner core must grow as the earth cools, forming a solid matrix containing a melt fraction in a layer on its outer boundary. Little is yet known about this process, which is still largely conjectural.

Examples of compaction and of two phase flow are also common in fields remote from Geology. In Materials Science especially, systematic investigations of the physical mechanisms involved in compaction have been carried out, and the processes involved are now reasonably well understood. Though this work has some relevance to the geological problem, the shape of individual pores depends on whether they are filled with melt, as they are in the mantle, or are empty, as they often are in engineering problems. Two phase flow also occurs in fluidized beds and forms the basis of the science of Hydrology. Again these problems are better understood than is that of magma extraction, and can provide

understanding of a variety of model problems which are simpler than the real geological problem, but which are relevant to it. It is, however, important to understand the physical processes involved in all these examples if they are to be helpful in understanding the geological problem. It is also important to start from differential equations which describe the conservation of mass, momentum and energy, since no one doubts that these constraints must be satisfied during the melting process.

TABLE 1

Notation

Variable	*Meaning*	*Value used*	*Dimensions*
a	particle radius	10^{-3}	m
$\mathbf{a}_z$	unit vector in vertical		none
C_p	specific heat at constant pressure	10^3	J kg^{-1} K^{-1}
C_p^f	specific heat of melt at constant pressure		J kg^{-1} K^{-1}
C_p^s	specific heat of matrix at constant pressure		J kg^{-1} K^{-1}
c_f	concentration by weight in the melt		none
c_s	concentration by weight in the matrix		none
D_{11}	horizontal diffusivity		m^2 s^{-1}
D_{33}	vertical diffusivity		m^2 s^{-1}
D_b	grain boundary diffusivity		m^2 s^{-1}
D_f	diffusivity of melt (Hofmann & Magaritz, 1977)	10^{-10}	m^2 s^{-1}
D_s	diffusivity of matrix (Hofmann & Hart, 1978; Miyamoto & Takeda, 1983)	10^{-17}	m^2 s^{-1}
g	acceleration due to gravity	9·81	m s^{-2}
H	rate of internal heat generation		J m^{-3} s^{-1}
h	depth of a layer		m
K_c	$= c_s/c_f$ partition coefficient between matrix and melt		none
k	Boltzmann's constant		J K^{-1}
k_T	effective thermal conductivity of melt and matrix equation (A38)		Wm^{-1} K^{-1}
k_T^f	thermal conductivity of melt		Wm^{-1} K^{-1}
k_T^s	thermal conductivity of matrix		Wm^{-1} K^{-1}
k_ϕ	specific permeability		m^2
$\mathbf{I}$	body force on the matrix from melt movement		N m^{-3}
L	latent heat of melting		J kg^{-1}
l	length scale		m
$\frac{D_v M}{Dt}$	the rate of conversion of matrix into melt/unit volume, measured in a frame fixed to the matrix		kg m^{-3} s^{-1}
P	pressure		Pa
P_f	pressure in melt		Pa
P_s	presure in solid		Pa
Ra	Rayleigh number for convection in a porous medium equation (3.9)		none
Re	$= \lvert\mathbf{v}\rvert l/\nu$ Reynolds number		none
S_f	entropy of the melt		J kg^{-1} K^{-1}
S_s	entropy of the solid		J kg^{-1} K^{-1}
ΔS	entropy change on melting	362	J kg^{-1} K^{-1}
T	absolute temperature		K
T_s	solidus temperature		K
ΔT	temperature difference between liquidus and solidus		K
t	time		s
t'	$= t/\tau_0$ dimensionless time		none
t_f	total melt thickness		km
$\mathbf{V}$	$= (U, V, W)$ velocity of matrix		m s^{-1}
$\mathbf{v}$	$= (u, v, w)$ velocity of melt in pores		m s^{-1}
ΔV	volume change on melting $= \left(\frac{1}{\rho_f} - \frac{1}{\rho_s}\right)$		m^3 kg^{-1}

Variable	*Meaning*	*Value used*	*Dimensions*
W'	$= W/w_0$ dimensionless vertical matrix velocity		none
w'	$= w/w_0$ dimensionless vertical melt velocity		none
w_e	transport velocity of solute, equation (5.3)		m s^{-1}
w_0	reference vertical velocity, the minimum fluidization velocity, equation (B7)		m s^{-1}
X	melt fraction by weight		none
x, y	horizontal coordinates		m
x' }	$= x/\delta_c$ dimensionless		none
y' }	$= y/\delta_c$ horizontal coordinates		
z	vertical coordinate, positive upwards		m
z'	$= z/\delta_c$ dimensionless vertical coordinate		none
α_f	thermal expansion coefficient of melt (Dane, 1941)	$6{\cdot}8 \times 10^{-5}$	K^{-1}
α_s	thermal expansion coefficient of matrix	4×10^{-5}	K^{-1}
γ_{sf}	grain boundary energy between matrix and melt		N m^{-1}
γ_{ss}	grain boundary energy between matrix grains		N m^{-1}
δ	grain boundary thickness		m
δ_c	$= \left[\dfrac{(\zeta + \frac{4}{3}\eta)}{\mu} k_\phi\right]^{1/2}$ compaction length		m
ζ	$= (1-\phi)\zeta^x$ effective bulk viscosity of matrix	10^{15}	Pa s
ζ^x	bulk viscosity of matrix		Pa s
η	$= (1-\phi)\eta^x$ effective dynamic shear viscosity of matrix	10^{15}	Pa s
η^x	shear viscosity of matrix		Pa s
Θ	dihedral angle, Fig. 4*a*	50°	
κ_T	effective thermal diffusivity of melt and matrix, equation (A40)	10^{-6}	m^2 s^{-1}
μ	dynamic shear viscosity of melt (Murase & McBirney, 1973)	1	Pa s
ν	$= \mu/\rho_f$ kinematic shear viscosity of melt		m^2 s^{-1}
ρ_f	density of melt	$2{\cdot}8 \times 10^3$	kg m^{-3}
ρ_s	density of matrix	$3{\cdot}3 \times 10^3$	kg m^{-3}
$\bar{\rho}$	$= (1-\phi)\rho_s + \phi\rho_f$ mean density of melt and matrix		kg m^{-3}
$\boldsymbol{\sigma}$	$\equiv \sigma_{ij}$ stress tensor		Pa
$\boldsymbol{\sigma}'$	$\equiv \sigma'_{ij}$ deviatoric stress tensor in matrix		Pa
$\boldsymbol{\sigma}^f$	$\equiv \sigma^f_{ij}$ stress tensor in melt		Pa
$\boldsymbol{\sigma}^s$	$\equiv \sigma^s_{ij}$ stress tensor in matrix		Pa
τ	a characteristic time		s
τ_0	reference time, characteristic time for compaction equation (B11)		s
ϕ	porosity of matrix		none
ϕ_0	initial porosity of matrix		none
ϕ_1	isolated porosity		none
Ω	Atomic volume		m^3
∇'	$= \delta_c \nabla$ dimensionless vector operator		none

2. THE GOVERNING EQUATIONS

The equations governing the conservation of mass, momentum, energy and each element individually are obtained in Appendix A. Those governing the conservation of melt and matrix separately are

$$\frac{\partial \phi}{\partial t} = -\nabla.\phi\mathbf{v} = \nabla.(1-\phi)\mathbf{V} \tag{2.1}$$

where ϕ is the volume fraction occupied by the melt, called the porosity, $\mathbf{v}$ is the mean velocity of the melt and $\mathbf{V}$ that of the matrix. An alphabetic list of all the variables used will be found in Table 1. Equation (2.1) applies only if the matrix does not melt. If it does then the melt and the matrix are not individually conserved.

The equation governing the difference in the velocity of the melt and matrix is a modification of D'Arcy's law

$$\mathbf{v} - \mathbf{V} = -\frac{k_\phi}{\phi\mu}\nabla(P + \rho_f g z) \tag{2.2}$$

where μ is the viscosity of the melt, k_ϕ the permeability, P the pressure ρ_f the density of the fluid and g the acceleration due to gravity, z is the vertical distance, taken to be zero on the surface of the layer and to be positive upwards. The factor ϕ dividing the right-hand side arises because k_ϕ is usually determined by measuring the average velocity with which a fluid passes through a permeable solid, and not the velocity of the fluid in the pores (see for instance Dullien, 1979, p. 78). This equation has been widely used in the geological literature, generally with the matrix velocity taken to be zero (Sleep, 1974; Ahern & Turcotte, 1979; Walker *et al.*, 1978; Stolper *et al.*, 1981). The physical meaning of the equation is that the flow is driven by the difference in the actual pressure P and the hydrostatic pressure $-\rho_f g z$. It is usually written down as an empirical law, though its form can be derived from the theory of two phase flow, as is done in Appendix A. The reason why it is useful to do so is that the force which the matrix exerts on the melt, which leads to (2.2), also acts on and can deform the matrix.

The equation which governs the motion of the matrix has not been found in the literature, and may be written in a variety of ways. It can also be obtained directly by a physically plausible argument. If the pressure is sufficient to support the weight of the overlying partially molten material, no compaction will occur. This condition is satisfied if the pressure gradient obeys

$$\frac{dP}{dz} = -\bar{\rho}g \tag{2.3}$$

where $\bar{\rho}$ is the mean density of the material:

$$\bar{\rho} = (1 - \phi)\rho_s + \phi\rho_f \tag{2.4}$$

and ρ_s is the density of the matrix. If (2.3) is not satisfied then the matrix will expand if

$$\frac{dP}{dz} + \bar{\rho}g > 0 \tag{2.5}$$

or compact if this expression is less than zero. Though the physical meaning of the equation governing compaction is clearest when it is expressed in terms of the pressure, it is generally more convenient to solve the equation when it is written in terms of $\mathbf{v}$ and $\mathbf{V}$, because the boundary conditions are generally given in terms of velocity, not pressure. When (2.3) is not satisfied and the matrix deforms, it probably does so like a viscous fluid, at least at low stresses. This behaviour arises because diffusion through the melt provides a means of changing the shape of the individual crystals of which the matrix consists, without deforming the crystals internally. Hence the viscosity of the matrix is an average property, and applies only to regions large enough to include a large number of crystals and pores. The deformation of viscous fluids whose density is constant can be described by the familiar shear viscosity η. If, however, the mean density of the porous matrix is not constant, as it is not in the problem considered here, two viscosities are required to describe the deformation, the shear viscosity and the bulk viscosity ζ (see Landau & Lifshitz, 1959, p. 48). These two constants are independent, though they can often be related to each other if deformation mechanism is understood. The bulk viscosity of a two phase system was calculated by Taylor (1954) for a

suspension of gas bubbles in a liquid. A similar calculation is carried out below to obtain the bulk viscosity of the matrix (Appendix C).

An expression similar to that derived here was proposed by Sleep (1974) for the deformation of the matrix. He, however, assumed that the bulk viscosity was zero. If this assumption were true the matrix would exert no resistance to isotropic compaction (see Appendix C). Such behaviour is implausible, and is not compatible with any of the proposed mechanisms which change the shape of individual crystals of the matrix (Artz *et al.*, 1983). Therefore the equations containing the bulk viscosity should be used.

Two other equations can be derived from the conservation of energy and of individual elements. The energy equation is complicated and contains a large number of terms. A detailed investigation of its solutions will require numerical experiments. The conservation equation for each element is simpler because source terms are absent.

Various important assumptions have been made in the derivation of the governing equations, all with the aim of producing equations which contain enough of the physics of the problem to be interesting while still remaining sufficiently simple to solve by standard methods. The first assumption is that the creep rate of the matrix depends linearly on the stress. Under the low stresses prevalent in the partially molten regions of the upper mantle this assumption is probably valid (Pharr & Ashby, 1983). It is certainly premature to attempt to use a more complicated rheology.

The second assumption is that the pressure in the melt is the same as that in the matrix, or that the surface energy of the matrix grains has no influence on the dynamical behaviour. Bulau *et al.* (1979) and Waff & Bulau (1979) have clearly demonstrated that the surface energy of the matrix controls the detailed morphology of the melt distribution. Drew & Segal (1971) discuss the inclusion of such surface energy terms in the momentum equations, but the resulting expressions appear to be somewhat intractable. It therefore seemed worthwhile to explore first the simpler system of equations in which the surface energy is neglected.

3. THE PHYSICAL PROCESSES INVOLVED IN COMPACTION

The melt fraction present in the mantle must vary with depth, since it is zero at the surface and presumably also at great depths. It is therefore of interest to examine how this variation affects the movement of the melt and matrix. The simplest model in which the melt fraction ϕ varies is one in which ϕ changes from zero to some constant value on a horizontal boundary $z = 0$. It is then easy to show that there is no solution to the equations if the velocities of the matrix and melt are both zero. If the melt velocity was zero the pressure would have to be hydrostatic

$$\frac{dP}{dz} = -\rho_f g \tag{3.1}$$

If, however, the matrix is not to deform by compaction, (2.3) requires

$$\frac{dP}{dz} = -[(1-\phi)\rho_s + \phi\rho_f]g. \tag{3.2}$$

(3.1) and (3.2) can only both be true if $\phi = 1$, which requires the matrix to be absent. For any other value of ϕ no solution can exist without compaction. This result was first pointed out by Waff (1980), but he did not believe that real partially molten rock behaved in this way. Instead he argued that the difference between the two pressure gradients (3.1) and (3.2) was maintained by surface forces, and therefore that the pressure within the fluid differs from that within the solid. He was then able to construct a non-uniform static distribution of melt

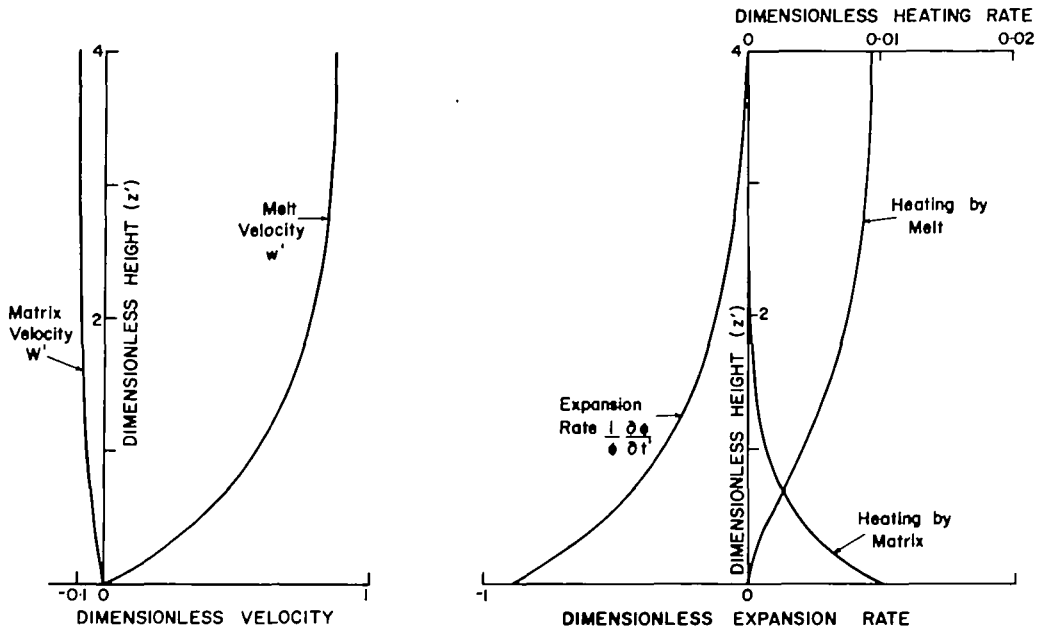

FIG. 1. (*a*) Dimensionless matrix velocity W' and melt velocity w' as functions of dimensionless height above an impermeable layer at $z' = 0$ (equations (B16) to (B18)) for $\phi = 0{\cdot}1$. The boundary condition at $z' = 4$ is that the stress on the matrix should be zero. Upward velocities are positive. (*b*) Dimensionless expansion rate, $1/\phi\,\partial\phi/\partial t'$, and dimensionless dissipative heating produced by the deformation of the matrix and movement of the melt corresponding to the flow in (*a*). All quantities have been scaled using (B25) to (B28).

and matrix. He did not examine the stability of his solution, nor did he explain how the proposed distribution could arise. Until clear geological evidence requires the existence of such static models it seems preferable to assume that they are not stable solutions to the problem.

The flow within a layer with a free upper boundary across which melt can flow, compacting onto an impermeable horizontal plane (Fig. 1; Appendix B) illustrates the general form of the behaviour. Both the velocity of the matrix W' and melt w' are dimensionless. In a layer near the lower boundary the upward velocity of the melt increases with height until it is sufficiently great to balance the pressure gradient produced by the mean density. Thereafter all the weight of the melt and matrix is supported by the upward percolation of the melt, and no compaction occurs. This behaviour is most clearly seen in the plot of the dimensionless expansion rate $1/\phi\,\partial\phi/\partial t'$, which is negative when compaction is occurring. Compaction occurs most rapidly at the base of the layer, and the rate decreases exponentially with height. This behaviour can be used to define the thickness of the compacting boundary layer. The characteristic length over which the compaction rate decreases by a factor e will be referred to as the compaction length, δ_c, and is given by

$$\delta_c = \left[\frac{\zeta + \frac{4}{3}\eta}{\mu} k_\phi\right]^{1/2} \tag{3.3}$$

where ζ and η are the bulk and shear viscosities of the matrix of permeability k_ϕ, and μ is the viscosity of the melt. As is demonstrated in Appendix A this length is a fundamental length scale of the problem, and will govern the behaviour of all compacting layers. The discussion in section 4 shows that the permeability can be written as $a^2 f(\phi)$, where a is the radius of the

grains making up the matrix and $f(\phi)$ is a function which depends only on the porosity. Hence

$$\delta_c = \left[\frac{\zeta + \frac{4}{3}\eta}{\mu} f(\phi)\right]^{1/2} a \tag{3.4}$$

and depends on the ratio of the viscosity of the matrix to that of the melt. It is scarcely surprising that both the viscosities of the melt and of the matrix are involved, because the melt can only be expelled if the matrix can compact. What is perhaps more surprising is that δ_c does not depend on the gravitational forces, since it is independent of g and $\rho_s - \rho_f$.

The example in Fig. 1 also allows the dissipation rate in the melt and matrix to be calculated. Dissipative heating occurs in the melt because it is flowing through the porous network formed by the matrix and in so doing generates heat. Heating by matrix deformation is restricted to the region in which compaction (or expansion) is occurring. It is of interest that the maximum rate of dissipation by each mechanism is the same. This result does not depend on the values of the viscosities of the melt and matrix, or on the porosity.

In the example shown in Fig. 1 the layer depth h is $4\delta_c$. An important limiting case occurs when $h \ll \delta_c$. The melt is then free to escape from the matrix, and the velocities and the compaction rate should be independent of μ and k_ϕ. The solutions to this problem when $h \ll \delta_c$ show that the velocities and compaction rate depend only on the expression

$$\frac{w_0}{\delta_c^2} \tag{3.6}$$

where w_0 is the relative velocity between the melt and matrix where no compaction is occurring

$$w_0 = \frac{k_\phi}{\mu} \frac{(1-\phi)}{\phi} (\rho_s - \rho_f) g \tag{3.7}$$

substitution of (3.7) and (3.3) into (3.6) gives

$$\frac{w_0}{\delta_c^2} = \frac{1-\phi}{\phi} \frac{(\rho_s - \rho_f) g}{(\zeta + \frac{4}{3}\eta)} \tag{3.8}$$

This expression therefore confirms the physical argument above, and shows that the velocities and compaction rate are independent of melt viscosity and the permeability. The resulting variation of the dimensionless velocities and expansion rate with dimensionless height in this case (Fig. 2) is rather different from the case when $h = 4\delta_c$ in Fig. 1.

These two examples demonstrate that the compaction is either controlled by the properties of both the matrix and the melt, or by those of the matrix alone, depending on the value of h/δ_c. No solutions exist in which the behaviour is controlled by the properties of the melt alone. It is therefore essential to take into account the deformation of the matrix when discussing the extraction of magma from a partial melt.

Two familiar examples illustrate that it is the value of h/δ_c, not h alone, which controls the behaviour of a compacting layer. The first is the behaviour of an oil–water mixture such as salad dressing. When this mixture is shaken and then left to stand, an oil layer forms at the surface in which the oil bubbles are separated by a small amount of trapped water. The upward motion of the oil and downward motion of the water are easily visible. Since the viscosity of the oil is small, though greater than that of water, $h/\delta_c \gg 1$, even though the physical size of the experiment is small.

The second example is the movement of water in a thick layer of sand. Many excellent aquifers consist of a sand horizon between less permeable shales. On a geological time scale a

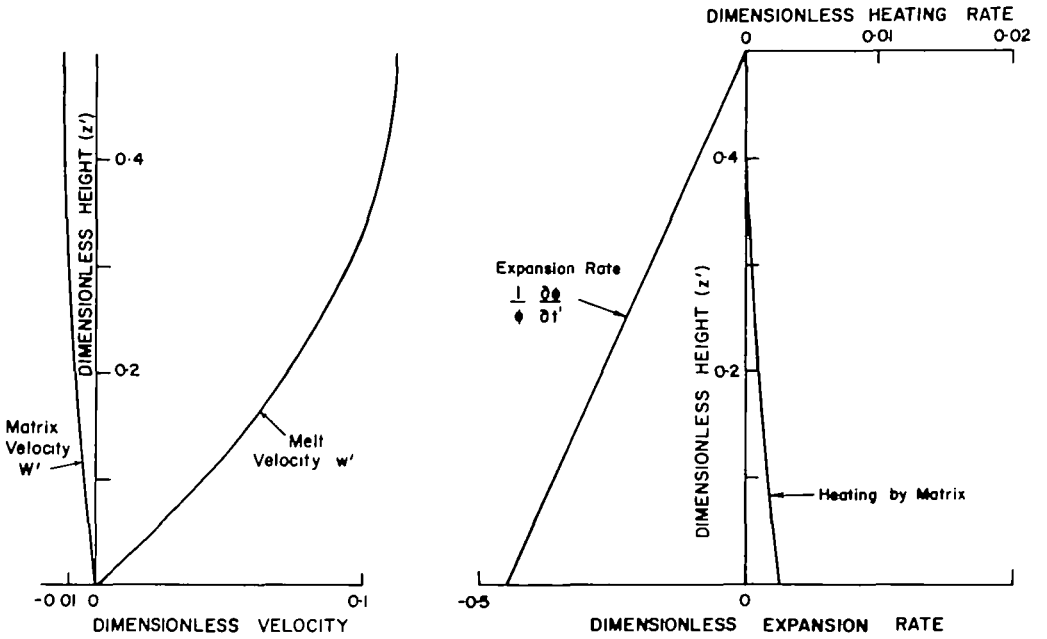

FIG. 2. (*a*)(*b*) As for Fig. 1, but for a layer whose depth is small compared with δ_c (equations (B21) to (B23)).

process known as pressure solution occurs in which the quartz dissolves in the water adjacent to the points of contact between the quartz grains and is redeposited elsewhere. This process allows the matrix to deform, but, because the solubility of quartz in water is small, it proceeds very slowly even in thick beds. Hence the effective viscosity of the matrix is large, and $h/\delta_c \ll 1$ even if the bed is 100 m or more thick. It is clear that the rate of compaction of the bed does not depend on the viscosity of the water or the permeability of the matrix, since such beds can act as aquifers.

The most striking feature of the solution in Fig. 1, with $h/\delta_c = 4$ is the existence of a region towards the top of the layer in which negligible compaction is occurring and the gravitational forces are supported by the upward percolation of melt. The relative velocity between melt and matrix in this region is w_0, given by (3.7), and is independent of the viscosities of the matrix. The existence of such a velocity is a well known feature of the two phase flow which occurs in fluidized beds, and is known as the state of uniform fluidization. It is also sometimes called the quick condition, since the behaviour of quicksands depends on the existence of an upward flow of water. There is, however, a considerable difference in the behaviour of fluidized beds and of partially molten rocks. Under most conditions the particles in fluidized beds are not deformable. Hence if the upward flow of fluid is sufficient to support the weight of the material the particles are free to move. It is this ability which gives such beds their fluid properties. Unless the melt fraction exceeds about 20 per cent (section 4), however, a partially molten rock consists of a network of interlocking grains. These will deform and expel melt if the melt velocity is less than w_0. Even if the velocity is greater than w_0 they still remain interlocked. Such a material will still possess a large viscosity η, controlled by the rate of deformation of the matrix, when deformed in shear.

A third solution illustrated in Fig. 3 has a different upper boundary condition from those in Figs. 1 and 2. Instead of a free upper boundary, both the matrix and melt velocities are required to be zero on both boundaries. The solution then has two boundary layers, both with a thickness comparable to δ_c. In the lower boundary layer compaction occurs to generate the

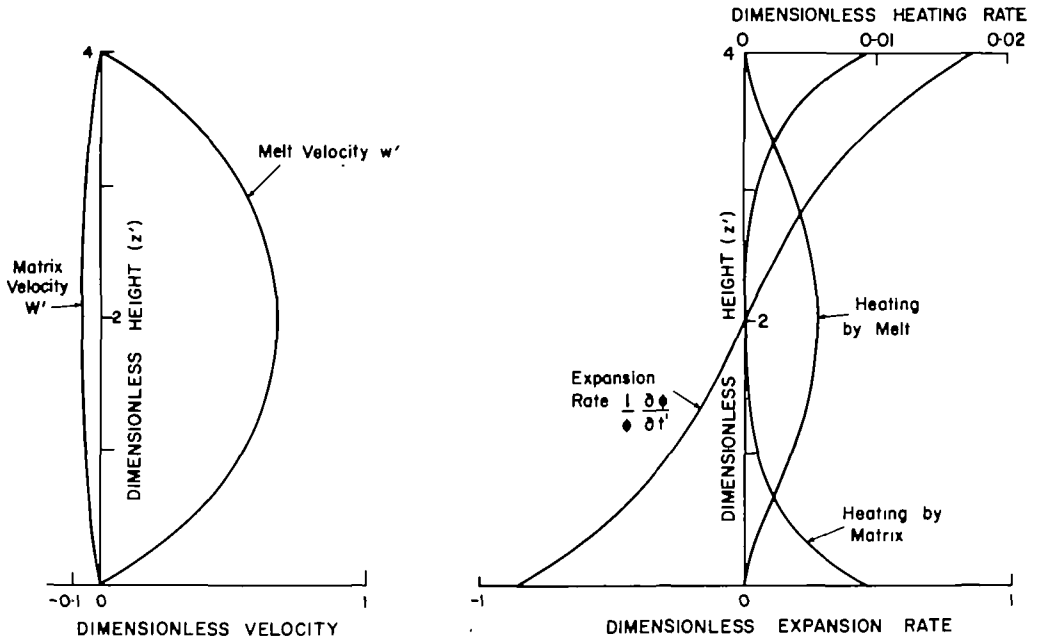

FIG. 3. (*a*)(*b*) As for Fig. 1, but with the matrix and melt velocities zero on both $z' = 0$ and 4 (equations (B12) to (B14)).

upward movement of the melt with relative velocity w_0. In the upper boundary layer expansion occurs to accommodate the melt expelled from the base layer. This solution is valid only if the grains of the matrix remain in contact, and the relevant conditions which must be satisfied are discussed in section 4. When, however, $\phi \lesssim 0{\cdot}2$ the grains will disaggregate and the solution will cease to be valid. Since the porosity increases most rapidly at the upper boundary, disaggregation will first occur there. When it does so a layer of pure melt will start to accumulate, and the upper boundary condition on the matrix will be that the stress, and not the velocity, is zero on the upper surface of the compacting layer. The solution will then be that shown in Fig. 1.

These solutions are valid only if the porosity is initially constant, and then only when $t = 0$. The governing equations can obviously be solved numerically to discover how the porosity varies with time as a function of z. No such integrations are carried out here, though a variety of solutions have been obtained (Richter & McKenzie, in preparation). It is also important to investigate whether the resulting solutions are stable. It is likely that stable solutions exist if both the initial porosity and permeability are monotonically increasing functions of z only, or are constant, though this result has not been proved. Two related problems have been studied which are known to be unstable. Saffman & Taylor (1958) showed that the displacement of a fluid filling the pores of a porous medium by another, less viscous, fluid results in fingering, with long tongues of the less viscous fluid penetrating into the medium. Preliminary results suggest that a similar type of instability occurs in the problem discussed above wherever the permeability decreases upward.

The other type of instability which may be relevant to the partial melt problem occurs in fluidized beds, and has been widely studied (Anderson & Jackson 1968, 1969; Homsy *et al.*, 1980; Didwania & Homsy, 1982; Liu, 1982). It occurs when the fluid velocity exceeds w_0, and takes the form of porosity waves travelling in the z direction. These waves may be unstable to transverse structures, and also to bubbling, in which bubbles of fluid form without

any particles (El-Kaissy & Homsy, 1976; Didwania & Homsy, 1981). Corresponding solutions probably exist to the partial melting problem.

Instabilities in compacting regions are likely to be of considerable importance in geological problems. The existence of igneous dykes is probably the expression of the instability which arises when the permeability decreases with height, and when the melt and matrix separate. The existence of diapirs of partially molten material suggest that there is another class of instability in which the melt and matrix move in the same direction. Certain sedimentary features are also likely to result from the same instabilities. Dyke-like bodies of sandstone are commonly found intruding an overlying less permeable shale, and are called neptunian dykes. The movement is believed to occur during the early stages of compaction, when the porosity of both sandstone and shale is large. The other observation which suggests instabilities are important is the occurrence of sand boils or volcanoes during earthquakes. In regions where the water table is shallow and saturated unconsolidated sediments occur, for instance in the flood plains of rivers, shaking produced by earthquakes produces fountains of a sand–water mixture from a series of vents. These two phenomena may well be related. Both suggest that the existence of a region of low permeability overlying a more permeable bed is unstable.

A rather different type of instability can arise from thermal buoyancy. If the vertical temperature gradient $\mathrm{d}T/\mathrm{d}z$ exceeds the adiabatic temperature gradient $(\mathrm{d}T/\mathrm{d}z)_s$ within the melt over a sufficiently large region, thermal convection can occur within the partial melt. The condition which must be satisfied is that the appropriate Rayleigh Number Ra defined by

$$Ra = \frac{g\alpha_f h^2 k_\phi \left[\dfrac{\mathrm{d}T}{\mathrm{d}z} - \left(\dfrac{\mathrm{d}T}{\mathrm{d}z}\right)_s\right] \rho_f C_p^f}{k_T(\mu/\rho_f)} \tag{3.9}$$

where k_T is the effective thermal conductivity given by (A38), α_f the thermal expansion coefficient of the fluid of density ρ_f and specific heat C_p^f, and h the depth of the layer, should exceed $4\pi^2$. Convection of the melt can then occur. Equation (3.9) assumes that horizontal temperatures gradients are absent. If they are present then thermal convection will occur irrespective of the value of Ra. However, the resulting velocities are small unless $Ra > 4\pi^2$.

At first sight the results obtained in this section may appear somewhat remote from the geological problem of partial melting. They certainly cannot be directly applied to, for instance, the movement of melt beneath a ridge axis. But a number of features of these solutions must be relevant to all regions where partially molten material exists. Compaction boundary layers must occur wherever the permeability changes. The mantle at sufficient depth is generally believed to be solid, so melting beneath ridges must produce compaction boundary layers. Where the lithosphere has formed by heat loss to the earth's surface, the permeability of the lithosphere must be less than that of the underlying asthenosphere. Here another boundary layer must form, which is probably unstable. Similar remarks apply to a partially solidified sill, which will also undergo compaction. Further progress in understanding all these problems will need to exploit the understanding provided by the simple solutions obtained above.

4. CONSTANTS IN THE GOVERNING EQUATIONS

Further progress requires estimates of the values of the various constants which enter the governing equations. Many of these are adequately known and are listed in Table 1 with references where necessary. But k_ϕ, η and ζ are not well determined, and all three depend on the detailed geometry of the melt phase.

Melting must first occur at the contacts between mineral grains of different composition. At

grain corners four different minerals may be in contact at a point, and the first melt will therefore be generated at these sites. If the melt remained there it would not form an interconnected network of pores and could not be extracted. However, simply because the melt is formed at grain corners does not mean it has to stay there. Whether it does so will depend on whether this configuration has the least energy, and if not, on how rapidly the pore geometry can be changed to achieve the minimum energy configuration. These questions are discussed in this section.

The rate at which the pore geometry can change by diffusion in a partial melt of basalt with an olivine matrix has been investigated by Vaughan & Kohlstedt (1982), who showed that equilibrium geometries are achieved in the laboratory in less than 200 h. The grain size used in these experiments was about 10 μm, and equilibrium will therefore be established more quickly than it will be in the geological problem, where the grain radius is around 1 mm. Nonetheless it is likely that the compaction time scale in the earth is sufficiently long for equilibrium to be reached. If, for instance, the time taken to do so depends on the square of the grain size, 1 mm grains will achieve an equilibrium geometry in less than 10^3 yrs. However, in other geological situations, such as the rapid transport of xenoliths by a basaltic magma, equilibrium geometry is probably not established (Maaløe & Printzlau, 1979). All the discussion below is based on the assumption that the pore geometry is in equilibrium, and is that of minimum energy. This important question should be examined by using laboratory experiments to determine the adjustment time as a function of grain radius and composition. If the adjustment time is short compared with the compaction time it should be possible to estimate the matrix viscosities by investigating the rate at which small perturbations to the equilibrium geometry decay.

The equilibrium geometry of two dispersed phases has been considered in some detail by Beeré (1975*a*, *b*), and some beautiful SEM photographs of pore shapes have been obtained (Beeré, 1981). The morphology is controlled by the ratio of the grain boundary energy between two grains γ_{ss} to that between a grain and the melt γ_{sf}. The forces at the point of contact between two grains and the melt must balance (Fig. 4*a*) and hence the dihedral angle Θ can be obtained by resolving the forces parallel to the grain boundaries:

$$\cos \Theta/2 = \gamma_{ss}/2\gamma_{sf} \tag{4.1}$$

As Beeré (1975*a*, *b*) shows, the value of Θ controls the geometry and stability of the pores. Provided $\Theta < 60°$ the pore space at the grain corners remains interconnected by pores along the grain edges at all values of the porosity ϕ. Furthermore small pores at the corners grow at the expense of large ones. Therefore regions of closed porosity do not form by collapse of the grain edge porosity, nor do the large pores grow at the expense of small ones. If, however, $\Theta > 60°$ there is a minimum value of ϕ which must be exceeded before an interconnected network of pores can exist. As Beeré (1975*a*) remarks, most liquids in equilibrium with solid grains have values of $\Theta < 60°$, and therefore the melt network will be stable. Furthermore he shows that such a network absorbs melt if placed in contact with a completely molten zone, a process which causes swelling. Such behaviour has also been observed in silicates by Watson (1982), who placed melt in contact with a basalt–peridotite analogue system and showed that the melt penetrated grain boundaries. The experiments of Waff & Bulau (1979) suggest that $\Theta \simeq 50°$ for a basalt-olivine system and therefore that the behaviour of silicate melts resembles that of other partially molten ceramics. This value of Θ was determined from SEM photographs and may not be very accurate. It is, however, likely that $\Theta > 0$, since Vaughan & Kohlstedt (1982) were unable to find melt on all grain boundaries.

The behaviour of the porosity networks when $\Theta > 60°$ is considerably different, as Beeré (1975*a*, *b*) shows. At low values of porosity closed pores are formed at grain corners, and the

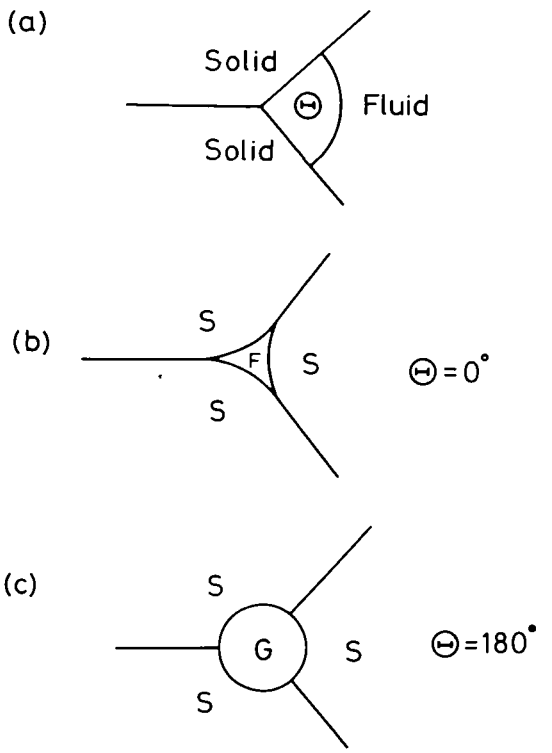

FIG. 4. (*a*) The angle between two grain-melt interfaces at a grain boundary is the dihedral angle Θ. (*b*) and (*c*) The shapes of the channels on grain edges depend on the dihedral angle. If the pores are occupied by melt (*b*) Θ is small and the boundaries concave, whereas if the pores are filled with gas or are empty, Θ is large and the boundaries convex.

larger pores are more stable than the smaller. Since all observations of silicate and other ceramic melts are compatible with $\Theta < 60°$, there is no reason to believe that such behaviour has geological relevance to the partial melting of mantle rocks. However, a great deal of experimental work on compaction has been carried out by materials scientists, with the pores either gas filled or evacuated. The compaction process is known as sintering when it takes place at atmospheric pressure and is driven by the reduction of surface area alone, and as hot isostatic pressing, or hipping, when a hydrostatic pressure is applied to the surface of the compacting material. When the pores are empty or filled with gas, Θ generally exceeds 60°. Therefore the pore geometry in such solids is rather different from that of partially molten materials, and results of sintering and hipping experiments may not be directly relevant to the behaviour of the matrix.

One important consequence of the melt network being a minimum energy configuration at all times is that its geometry is independent of whether the material is compacting or expanding. Hence the equations obtained in Appendix A should be valid in either case. Furthermore, since Waff & Bulau (1979) have determined a value of Θ of about 50° for silicate melts, Beeré's (1975*a*) curves can be used to estimate that disaggregation will not occur until $\phi \lesssim 0{\cdot}2$. As is shown in the next section, such large values of ϕ are not likely to occur in partial melts produced by mantle processes. Therefore the equations in Appendix A are likely to provide a good description of the dynamics of such material inside the earth. It is perhaps worth pointing out that similar arguments do not apply to the grain geometries of compacting sediments.

This discussion suggests that the permeability and matrix viscosities should be taken to be a function of Θ, as well as of ϕ and the grain radius a. The inclusion of both a and Θ as independent variables takes some account of Hashin's (1964) concern that the geometry of the matrix and melt must affect the material constants. In most mixtures there is no single variable controlling the geometry of the phases, and therefore the behaviour of partially molten material may for this reason be simpler to analyse than that of most composite materials.

The other important conclusion which follows from this discussion is that the melt will not remain at the sites where it is produced but will be distributed along all the grain edges to form an interconnected network.

One further remark which should be made at this stage is that the surface forces which control the melt geometry were neglected in deriving the governing equations. As Watson (1982) has shown, on a small scale this approximation is not valid. It is possible, but probably unlikely, that these forces are important on a large scale. Their principal effect is probably to control the melt network, which indirectly has a major influence on the large scale motions.

If the pore geometry is interconnected and stable, all regions of porosity will contribute to the permeability k_ϕ. Ahern & Turcotte (1979) and Maaløe & Scheie (1982) do not accept this argument, and have proposed that the isolated porosity ϕ_1 can be taken into account by allowing k_ϕ to be a function of $\phi - \phi_1$ rather than ϕ. The discussion above does not support this proposal. Isolated porosity forms at grain corners when $\Theta > 60°$. As the porosity increases this pore space will become part of the interconnected network, and when it does so its porosity should be included in the permeable porosity. Hence at sufficiently large values of ϕ all pore space will be permeable and the permeability will be independent of ϕ_1. Therefore their proposal is not likely to provide a satisfactory description of k_ϕ. Fortunately this question is unlikely to be important, because all available evidence indicates that the porosity network will remain interconnected at all values of ϕ.

The variation of k_ϕ with ϕ has been widely investigated, principally because it governs the flow of water and oil in porous rocks. Models of viscous flow in networks and measurements of the permeability of porous beds show that

$$k_\phi \propto a^2 \tag{4.2}$$

where a is the radius of the grains (see Bear (1972), fig. 5.5.1). The dependence of k_ϕ on porosity is more controversial. Dullien (1979, p. 161) lists a variety of proposed relationships and suggests that Rumpf & Gupte's (1971)

$$k_\phi = \frac{\phi^{5\cdot5} a^2}{1\cdot4} \tag{4.3}$$

agrees best with observations made on porous beds of randomly packed spheres with porosities between 0·35 and 0·65. These porosities are considerably greater than those which are likely to exist within the earth, and the geometry of the pores must also be different. Another relationship which has been proposed is

$$k_\phi = \frac{\phi^3 a^2}{K(1-\phi)^2} \tag{4.4}$$

and is often known as the Blake–Kozeny–Carman equation (Dullien, 1979). The constant factor K can be adjusted to match experimental observations. The value of K given by Bear (1972) is 45, but the predicted values of k_ϕ exceed those measured by Maaløe & Scheie (1982) by more than an order of magnitude at small values of ϕ. Therefore a value of K of 1000 was chosen to fit Maaløe and Scheie's measurements (Fig. 5).

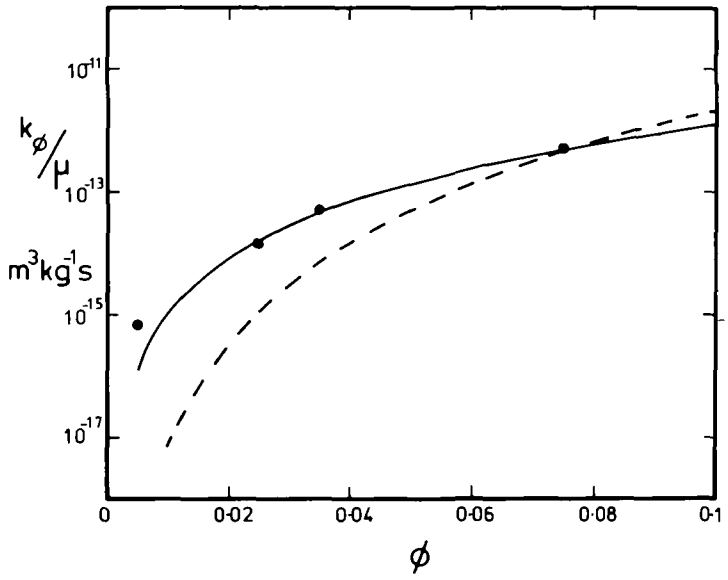

FIG. 5. The ratio of the permeability to the melt viscosity as a function of the porosity for a grain radius of 1 mm and a viscosity of 1 Pa s, obtained from equation (4.3), shown as a dashed line, and (4.4), shown as a solid line. The dots show Maaløe and Scheie's observations converted to the same grain radius using (4.2).

The variation of k_ϕ with ϕ is very rapid at low porosities no matter which expression is used. Fig. 5 shows curves of k_ϕ/μ for $a = 1$ mm and $\mu = 1$ Pa s, together with Maaløe & Scheie's values converted to the same grain size using (4.2). The plot shows that k_ϕ may change by as much as a factor 10^5 between $\phi = 0{\cdot}1$ and $0{\cdot}01$. As has previously been emphasized (Frank, 1968; Sleep, 1974; Ahern & Turçotte, 1979), this variation dominates the movement of melt through the matrix in the absence of compaction. Whether it does so also in the compacting layer depends on the behaviour of ζ and η.

Little is yet known about the variation of either the bulk viscosity or the shear viscosity with ϕ. Artz *et al.* (1983) have developed a theoretical microscopic model which can successfully account for compaction rates observed during hipping and the vertical compaction of ice. Their equation for the compaction rate when $\phi < 0{\cdot}1$ can be used to obtain an expression for $\zeta(\phi)$ (Appendix C). Fig. 6 shows that ζ varies by about a factor of 3 over the range $0{\cdot}1 > \phi > 0{\cdot}02$. The value of ζ cannot be estimated from (C12) because the relevant constants have not been determined. It is unlikely that the shear viscosity η varies as rapidly with ϕ as does ζ.

The expressions obtained by Artz *et al.* (1983) do not include the influence of the partial melt on the compaction rate, nor are the spherical pores at grain corners, which they use to obtain $\partial\phi/\partial t$ when $\phi < 0{\cdot}1$, likely to be a good approximation to the interconnected porosity of a partial melt with $\Theta < 60°$. The existence of a melt phase is very widely used to increase the densification rate during sintering, though the mechanism by which it does so is rarely well understood. Several investigations have demonstrated a considerable increase in compaction or creep rate as the temperature crosses the solidus. Bowen *et al.* (1976) found that the sintering rate of silicon nitride, which contained silica as an impurity, was proportional to the concentration of MgO which they added. They also showed that the activation energy changed at the lowest temperature at which the system MgO–SiO_2 could form a liquid. The change in activation energy is presumably caused by a change in the mechanism by which the sintering occurs. Podob (1977) hipped Astroloy powder below and above and solidus of the

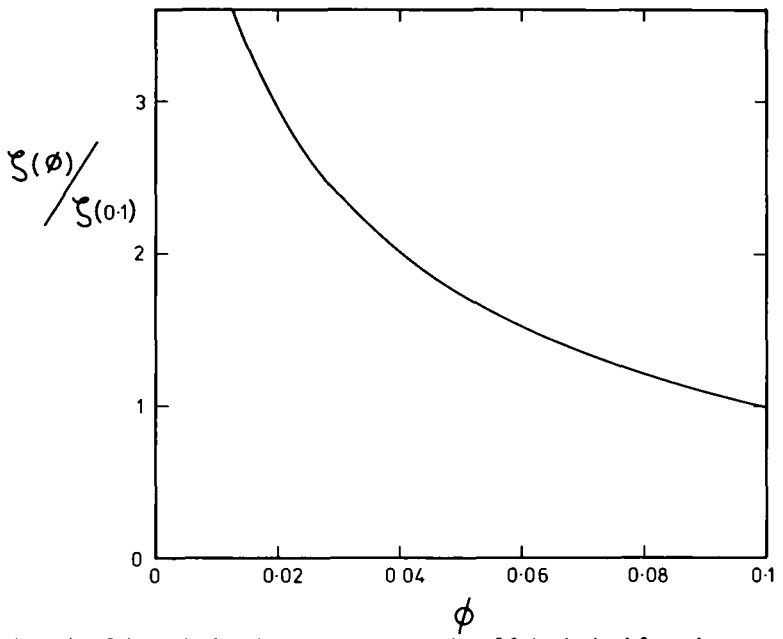

FIG. 6. The ratio of the bulk viscosity to that at a porosity of 0·1, obtained from the expression of Artz *et al.* (1982) (equation (C12)).

γ' phase, Ni_3 (Al, Ti), and showed that the resulting grain boundary structures were different. However, he did not measure the compaction rate. Verrall & O'Connell (1981) measured the creep rate of porous halite cylinders saturated with brine, and showed that the creep rate decreased by several orders of magnitude when the temperature decreased below the solidus of hydrohalite at 0·1 °C. One mechanism by which the creep rate can be increased by a second phase has been studied in detail by Gessinger & Fischmeister (1972). They showed that the increase in sintering rate of tungsten in the presence of a small amount of nickel is not produced by a continuous film of melted nickel, but by the migration of nickel to grain boundaries where it increases the diffusion rate of tungsten by about three orders of magnitude. This behaviour occurs whenever the temperature is sufficiently high for the nickel to migrate, and does not require melting. Perhaps the most useful experiments on the influence of a melt phase on the creep rate were carried out by Pharr & Ashby (1983) on creep in porous KCl and sugar. They compressed cylinders of KCl along their length whose pores were filled with a saturated solution of KCl in water–methanol mixtures, and showed that the creep rate is proportional to the solubility of the salt in the pore fluid. They also found that the creep rate is proportional to the stress, and depends on the temperature through an activation term with an activation energy of 19 kJ mol^{-1}. Sugar cubes behaved in a similar way. These results are similar to those of Verrall & O'Connell (1981), who carried out a less extensive series of experiments on NaCl. The principal difference is in the stress dependence. Verrall & O'Connell found that the creep rate depended on $\sigma^{1\cdot8}$, where σ is the stress, rather than the linear dependence of Pharr & Ashby. Neither of these experiments determined the dependence of the creep rate on grain size. Creep experiments have also been carried out at high temperature on a β-spodumene by Raj & Chung (1981) using three point bending. They showed that the creep rate was proportional to the stress and to the reciprocal of the grain size.

The principal problem with all these experiments is that they cannot be used to determine ζ and η independently, nor can they determine the variation of either with porosity.

Experiments like those of Pharr and Ashby could do so if the rate of increase in the diameter of the KCl cylinders is measured, as well as their longitudinal strain rate (Appendix C). It may, however, be better to measure ζ and η independently. ζ can be determined from the radial strain rate of a porous sphere enclosed in a membrane from which the fluid is allowed to escape. The rate of contraction can be determined by measuring the rate of loss of fluid (Appendix C). The shear viscosity can be measured by twisting a hollow cylinder, where the couple is transmitted to the cylinder by the means of teeth at each end, in the same way as Kamb (1972) deformed ice. The experiments should aim to determine dependence of ζ and η on the grain size and porosity, as well as on the variables investigated by Pharr and Ashby, and should also involve detailed examination of the resulting microstructure of the matrix.

An obvious alternative to laboratory measurements of ζ and η is to use geological observations to estimate their values within the earth. There are a number of areas where partially molten rock is likely to be present at depth from which estimates of the viscosity can be obtained. One such region is the Basin and Range, where Lake Bonneville provided a water load during the Pleistocene which has since evaporated. Crittenden (1963) estimated the viscosity to be 10^{20} Pa s, or a factor of ten less than that from Fennoscandia where little melt is likely to be present. Estimates from the shape of the axial valley (Sleep, 1969) and the thermal instability of the thermal boundary layer beneath plates (Parsons & McKenzie, 1978; Houseman & McKenzie, 1982) all lie between 10^{18} and 10^{20} Pa s. Discussion of the force balance on plates (Richter & McKenzie, 1978) also yields similar values for a thin low viscosity layer which is required to decouple the plates from the mantle below. All these estimates are of the shear viscosity η, and none is yet available for ζ. Useful estimates of $(\zeta + \frac{4}{3}\eta)$ can perhaps be obtained from studies of thick basic sills whose cooling time can be calculated. The extent to which the olivine, which has crystallized from the melt, has compacted may provide a better estimate of the matrix viscosity than do any larger scale geophysical measurements.

It is clear from this discussion that values of ζ and η for the matrix of partial melts are at present unknown. It is, however, clear that the situation can be improved considerably by carrying out a number of simple experiments. It is also clear that geophysical observations imply that the matrix viscosity is likely to be reduced by a factor of at least 10^3 by the presence of melt. Verrall & O'Connell (1981) found a reduction by a factor of at least 10^6. A value of 10^{15} Pa s is therefore used for ζ, η and all combinations thereof, such as $(\zeta + \frac{4}{3}\eta)$. Dependence of these viscosities on porosity, grain size and dihedral angle will be ignored. Clearly such a procedure is unsatisfactory. But until detailed experiments have been carried out and interpreted with a simple microscopic theory, any other procedure will suggest a spurious accuracy.

5. GEOLOGICAL APPLICATIONS

The composition of a magma erupted at the surface depends on the composition of the source material, the extent to which it melted, how much of the melt was extracted and how it was affected by fractionation and other processes on its way to the surface. All these phenomena must be understood if the composition of the magma is to be used to determine that of its source rock. The investigations in the previous sections can be used as a guide to all but one of these processes, the exception being fractionation.

Melt generation

The amount of melt is commonly estimated from some proposed geotherm by superimposing the geotherm on a phase diagram of, for instance, a garnet peridotite. This procedure is valid only if the geotherm is controlled by thermal conduction. If the temperature

is dominated by thermal convection, then the geotherm is controlled by the temperature of the upwelling material before it reaches the solidus and by the variation of melt fraction with pressure and temperature. Bickle & McKenzie (in preparation) have examined whether the heat transport by magma percolation is likely to dominate the conductive heat transport, and find that it will do so in all places where appreciable volumes of magma are being erupted. Therefore, except within about 5 km of the surface, conductive heat transport is of little importance and can be neglected.

The equation governing the conservation of energy (Appendix A) is the most complicated of all the conservation equations, and therefore it is important to investigate simplified models before attempting to understand geological problems. Somewhat surprisingly, these can be used to obtain reasonably accurate estimates of the fraction of the rock which melts during upwelling, and the volume of magma which will be erupted. Furthermore the relevant equation is sufficiently simple to allow solutions to be obtained for geologically important rock compositions.

The assumptions which are required to produce such a model are that the melt and matrix do not move relative to each other during partial melting of the rock, and that heat conduction and heat generation by viscous dissipation in the melt and matrix can be neglected. It is, however, straightforward to estimate how the relative movement affects the solutions, and, as is demonstrated below, the effects are comparable with the uncertainty in the latent heat of melting.

If there is no movement between the melt and matrix, the partially molten material will rise towards the surface at constant entropy, or isentropically. This result follows from the definition of entropy, and can also be obtained from the full equation governing the conservation of energy (Appendix D). As solid material rises it will first meet the solidus and start to melt. Since most rocks are not monominerallic, melting will occur over a temperature range. The simplest example is one in which the difference in temperature ΔT between the solidus and the liquidus is constant, and the solidus T_s is a linear function of pressure. If the latent heat of melting is known it is then straightforward to integrate the equation governing the conservation of energy to obtain the variation in melt fraction with depth if the melt and matrix are not allowed to move with respect to each other. An example is shown in Fig. 7, and illustrates the paths followed for various initial temperatures. As the material upwells it meets the solidus and starts to melt. Its temperature then decreases more rapidly than it does along either the solid or the liquid adiabats, because heat is absorbed by the melting process. The variation of melt fraction with temperature (Fig. 7*a*) shows that substantial quantities of melt can be present by the time the material reaches the surface. Once the porosity as a function of depth has been calculated, the total amount of melt produced by isentropic upwelling can be obtained by integration. This is shown in Fig. 7*c* in kilometres for each path. If such calculations are to be useful they must provide reasonably accurate estimates of the amount of melt generated, and that likely to be erupted. The amount which is likely to remain within the matrix is discussed below, and is probably less than 3 per cent. Therefore the melt will move with respect to the matrix as melting occurs, and accurate modelling will require the full energy equation to be solved. The effect of retaining 3 per cent of the melt within the matrix on the volume of melt which can be extracted is shown in Fig. 7*c*.

It is possible to estimate how important motion between melt and matrix will be from simple physical arguments (Appendix D). Movement of the melt has two major effects: it transports heat towards the surface and releases gravitational potential energy. The first effect occurs because the melt temperature falls less than that of the melt and solid in equilibrium during isentropic ascent. Hence the melt can melt some matrix as it ascends. The release of gravitational energy occurs because the melt density is less than the matrix. This difference

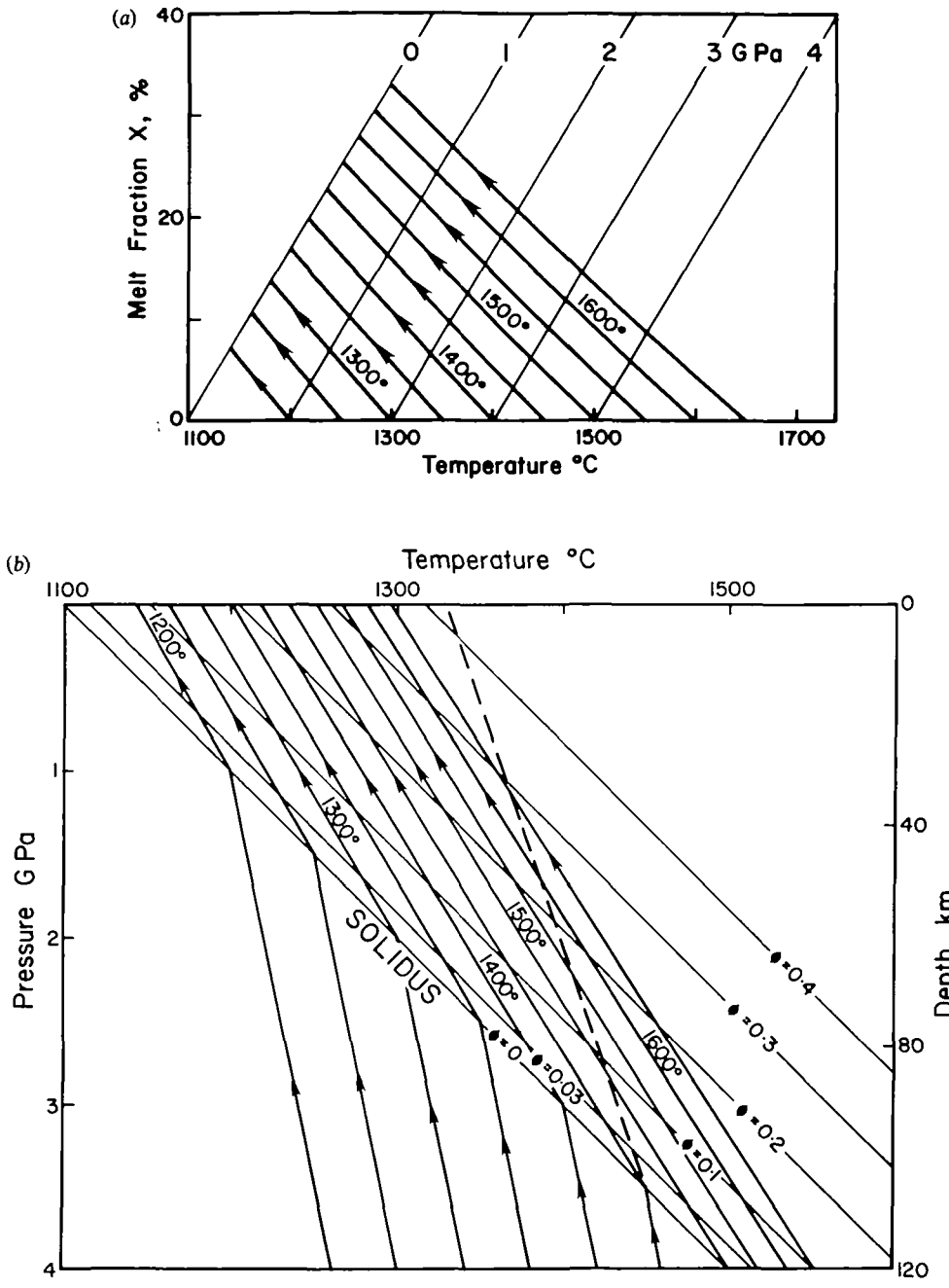

FIG. 7. (*a*) Melt fraction by weight X as a function of temperature for a number of isentropic melting paths (heavy arrowed lines) obtained by integrating (D7) and (D8) with $\Delta S = 362$ J kg^{-1} K^{-1}. The fine lines mark isobars, with the pressure marked in GPa. (*b*) The variation of temperature with depth (heavy solid lines) followed by rock upwelling at constant entropy, obtained by integrating (D7) and (D8). The continuous fine lines join points at which ϕ = constant. The change in gradient of the heavy lines occurs where melting starts. The dashed line shows the path of the melt alone upwelling at constant entropy. The temperatures marking the heavy lines are those at which they cross the solidus. (*c*) The continuous lines show the total volume of melt present below a given depth, obtained by integrating (D9). The dashed lines illustrate the amount of melt which can be extracted if 3 per cent remains in the matrix. The temperatures marking the lines indicate the temperature on the solidus.

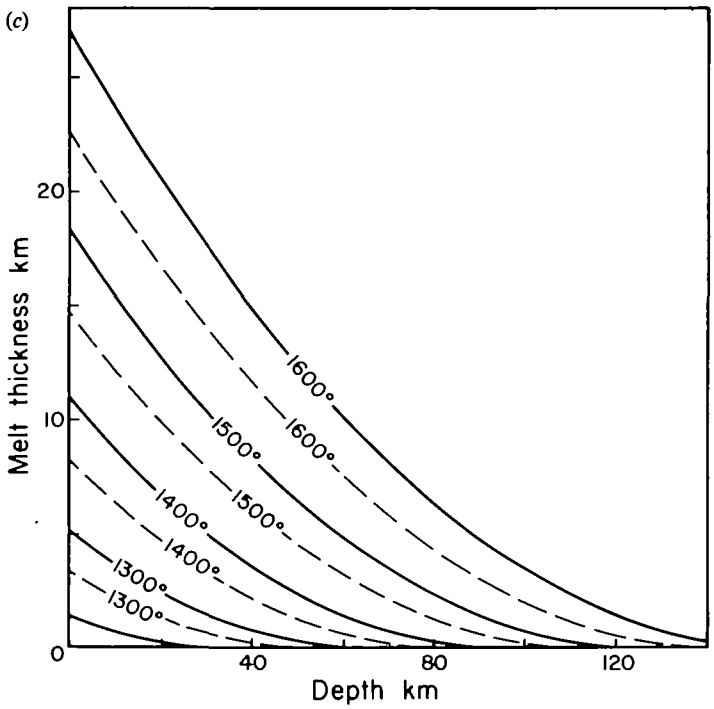

FIG. 7. (continued)

leads to viscous dissipation during the ascent of the melt, and hence also increases the amount of melting. Fig. 8 shows the effect of including the two additional sources of heat on the total thickness of melt generated. These changes can be compared with that produced by changing the latent heat of melting at 1350 °C from 590 kJ kg^{-1} to 400 kJ kg^{-1} (140 cal gm^{-1} to 100 cal gm^{-1}). Such a change is within the uncertainty of the present estimates of the latent heat, and has a comparable effect to the non-isentropic effects. Therefore isentropic upwelling should provide useful estimates of the amount of melting, and of the volume of melt produced at the surface. It will not, however, provide accurate estimates of the porosity variation with depth, or of the composition of the melt.

Further progress towards a useful geological model for melting during isentropic upwelling depends on obtaining empirical estimates of ΔS, the entropy difference between solid and liquid/unit mass, and the variation of melt fraction by weight, X, with pressure and temperature. Probably the best available estimate of ΔS is that made from $T_s(P)$ and the change in volume ΔV on melting. A recent determination of $T_s(P)$ for a garnet peridotite by Takahashi & Kushiro (1983) in Fig. 9 shows that a straight line with a gradient of 120 °C/GPa fits their observations well. As they point out, the shape of the solidus should depend on the phases present in the matrix. However, the difference between the straight line in Fig. 9 and their proposed solidus is considerably less than that between their curve and that of Mysen & Kushiro (1977); therefore their observations are probably adequately represented by a straight line. The value of ΔS can then be obtained from the thermodynamic relationship between dT/dP on the solidus and the volume change/unit mass ΔV

$$\frac{dT}{dP} = \frac{\Delta V}{\Delta S} \tag{5.1}$$

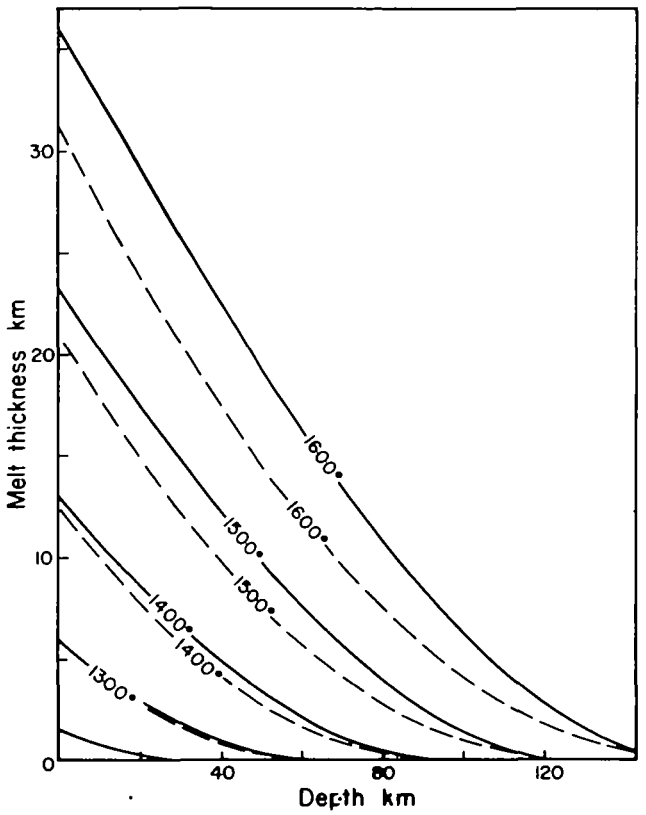

FIG. 8. The continuous lines show the total amount of melt generated when the heat transport by the melt and the gravitational energy released are taken into account, and $\Delta S = 362$ J kg^{-1} K^{-1}. The dashed lines show the melt generated by isentropic upwelling when $\Delta S = 250$ J kg^{-1} K^{-1}. The temperatures marking the lines indicate the temperatures on the solidus.

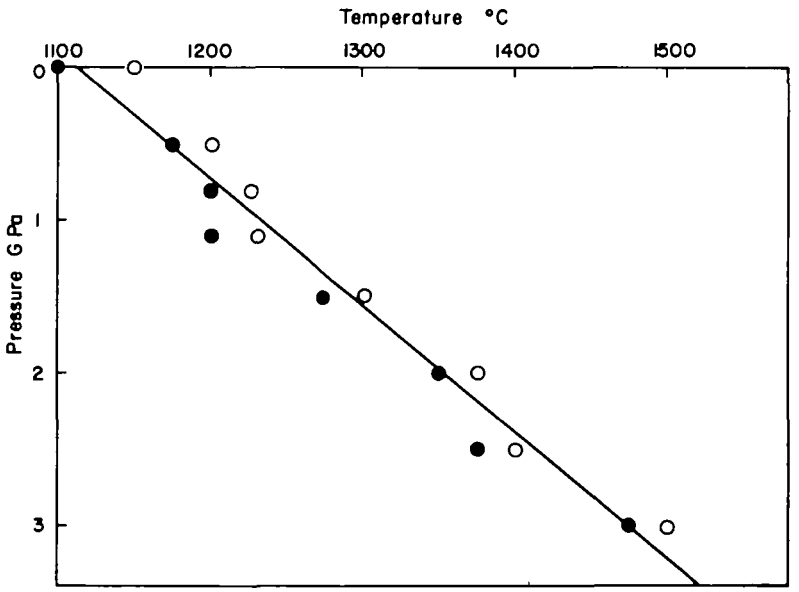

FIG. 9. The determination of the solidus by Takahashi & Kushiro (1983). Open circles correspond to runs in which melt was produced, closed circles ones in which no melting occurred. The straight line corresponds to $(T - 273) = 1115 + 120P$ where P is in GPa.

Taking $dT/dP = 120$ °C/GPa and $\Delta V = 4{\cdot}34 \times 10^{-5}$ m^3 kg^{-1} (Herzberg, 1983) gives $\Delta S = 362$ J K^{-1} kg^{-1}. This estimate cannot be regarded as accurate and may be in error by more than 20 per cent. It is not yet possible to estimate how ΔS will vary with the pressure and melt composition. The variation of melt fraction with pressure and temperature for garnet peridotite has, however, been determined by Mysen & Kushiro (1977) and by Jaques & Green (1980) by two different methods. The principal difficulty with both methods is the problem of crystal growth during quenching. Both sets of experiments, which are plotted in Fig. 10, may have underestimated X. An obvious feature of these results is the major change in behaviour which occurs between 1·5 and 2 GPa. It is probably produced by the different methods used by the two groups. It is not difficult to produce an empirical expression for $T(X, P)$ which agrees well with the observations (Appendix D, Fig. 10) and hence to obtain isentropic melting paths (Fig. 11*a*, *b*) and melt volumes corresponding to these experimental results. Though these curves differ in detail from those in Fig. 7, Takahashi & Kushiro's (1983) results disagree with those of Mysen & Kushiro by about 100 °C, and therefore it is not clear that the differences between Fig. 7 and 11 are outside experimental error. Furthermore the shape of the solidus in Fig. 11*b* is improbable, and disagrees with that in Fig. 9. Its curious shape is the result of attempting to fit both sets of experimental results to a single expression between 1·5 and 2 GPa. Hence the complicated expression for $T(X, P)$ given in Appendix D may be unrealistic. The calculations were therefore repeated using

$$\begin{aligned}(T - 273) &= 1115 + 120P + (600 - 136P)X, \quad P < 3{\cdot}5 \text{ GPa} \\ &= 1115 + 120P + 124X, P > 3{\cdot}5 \text{ GPa}\end{aligned} \tag{5.2}$$

where T is the temperature in K, P the pressure in GPa and X the melt fraction by weight. This expression corresponds to a linear decrease in the temperature, ΔT, between solidus and liquidus with pressure, from 600 °C at zero pressure to 124 °C at 3·5 GPa. This behaviour is similar to that seen experimentally, though it differs in detail. It also is consistent with Herzberg's (1983) argument that ΔT for a garnet peridotite should decrease with pressure. The isentropic upwelling curves for (5·2) in Fig. 12*a* differ little from those in Fig. 7 and 11.

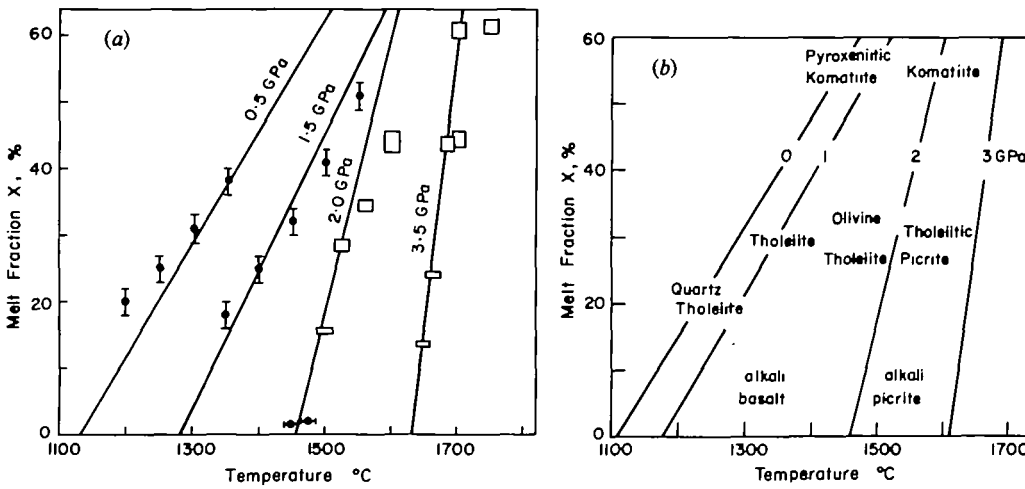

FIG. 10. (*a*) Solid circles with vertical error bars show determinations of $X(T, P)$ by Jaques & Green (1980) at 0·5 and 1·5 GPa for 'pyrolite', open rectangles and circles with horizontal error bars similar measurements by Mysen & Kushiro (1977) using a garnet peridotite of almost the same composition as the 'pyrolite'. The continuous lines show isobars obtained from the empirical expression (D15) designed to fit the experimental observations. (*b*) Melt compositions as a function of T and X from Jaques & Green (1980). The isobars were obtained from (D15), as in (*a*).

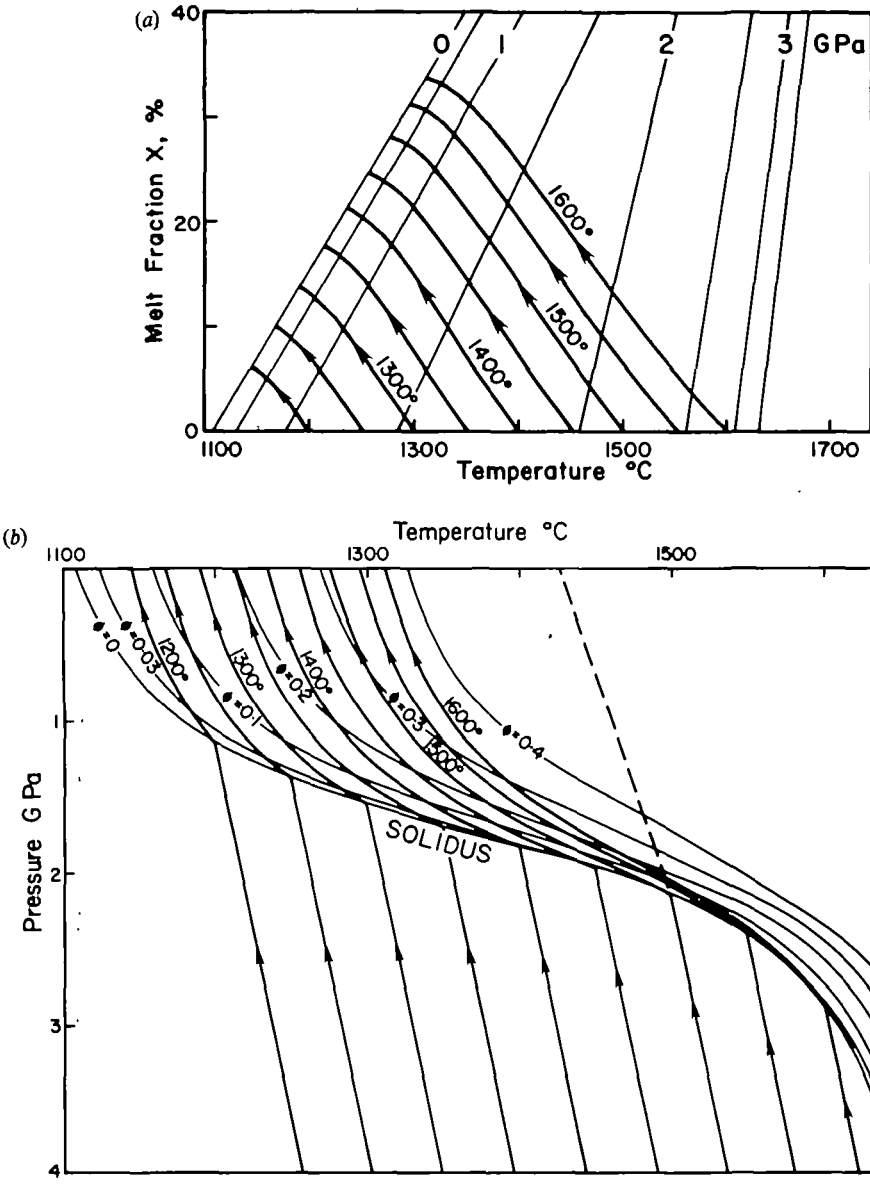

FIG. 11. (a)(b)(c) Isentropic melting paths like those in Fig. 7, but obtained using (D15) instead of (D8), with $\Delta S = 362\ \mathrm{J\ kg^{-1}\ K^{-1}}$.

A useful test of these melting calculations is to examine whether they are compatible with the relevant geological observations. Most melting occurs beneath ridge axes. Since there is no evidence of any association between ridges and upwelling limbs of convection cells, adiabatic upwelling of the mantle material whose temperature is the mean temperature of the mantle should be capable of producing oceanic crust 6 km thick. If the mean temperature is 1350 °C, Fig. 12*c* shows that upwelling can produce about 7 km of melt. A temperature of 1350 °C is compatible with other geophysical evidence (Parsons & Sclater, 1977) and the melt will emerge at a temperature of about 1210 °C, which is also reasonable.

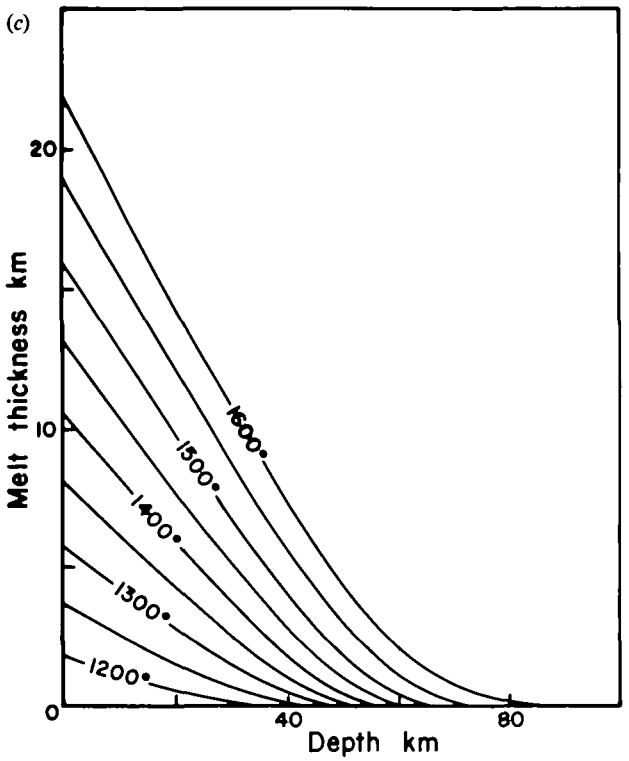

FIG. 11. (continued).

Convection within the mantle is driven by lateral temperature variations. Houseman (1983) has demonstrated that spreading ridges will travel across the surface of the convection pattern and leave it relatively undisturbed. Numerical models of mantle convection show that the probable magnitude of the temperature variations in the hot rising jets is no more than 200 °C above the mean temperature. Therefore the temperature of material rising into the melting region may be as great as 1550 °C when the ridge is on top of a hot rising region. As Fig. 12*c* shows, such an increase in temperature has a considerable effect on the volume of melt produced, and hence the crustal thickness over the hot regions should be between 20 and 25 km. Such values are in good agreement with seismic estimates of the crustal thickness beneath the Iceland–Faeroe Ridge (Bott & Gunnarsson, 1980), the Afar region (Berckhemer *et al.*, 1975; Ruegg, 1975) and the Madagascar Ridge (Goslin *et al.*, 1981; Sinha *et al.*, 1981), all of which are believed to be the result of ridge axis vulcanism when the ridge axis was on top of a hot rising region in the mantle.

The other environment where major effusions of magma occur is remote from plate boundaries. In oceanic areas major volcanic edifices such as Hawaii are built rapidly on old lithosphere. The gravity, geoid and residual depth anomalies (Watts, 1976; McKenzie *et al.*, 1980) show that the volcanism is at the centre of a larger region of positive residual depth and geoid anomalies which resembles that which is expected above a hot rising jet in the mantle. It is therefore of interest to examine whether the quantity of melt produced by such a jet is sufficient to account for the size of the Hawaiian ridge. The approximate width of the ridge is 100 km and its crustal thickness is 20 km. Therefore the cross sectional area of the ridge is about 2000 km^2, and it is being transported at a rate of about 100 mm yr^{-1} (Minster & Jordan, 1978) relative to the melting region by the motion of the Pacific plate. The output rate

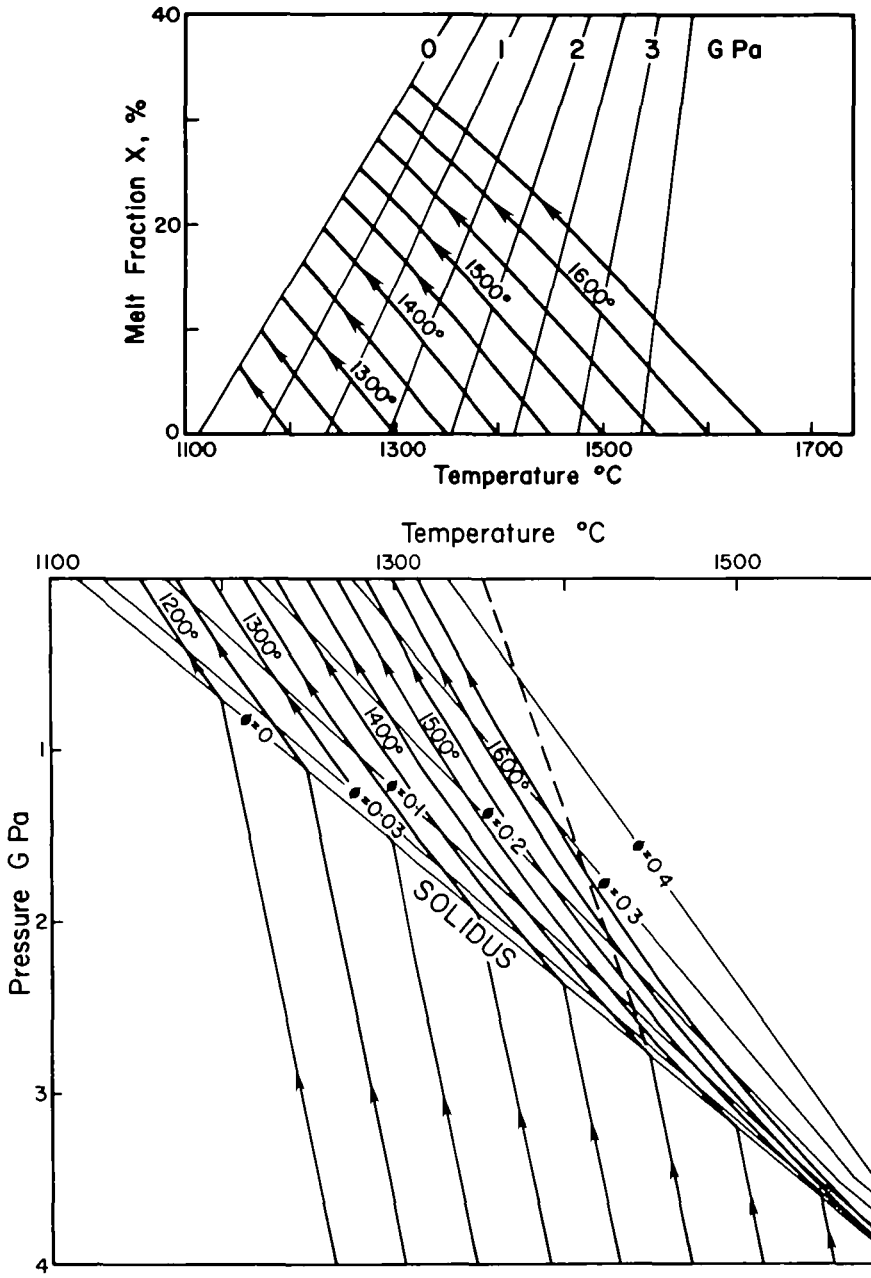

FIG. 12. (*a*)(*b*)(*c*) Isentropic melting paths like those in Fig. 7, but obtained using (D16) instead of (D8) with ΔS = 362 J kg^{-1} K^{-1}.

is therefore about 2 × 10^8 m^3 yr^{-1} or 6 m^3 s^{-1}. This estimate is about an order of magnitude greater than that of Wadge (1980), who considered only the volume erupted at the surface. This difference suggests that most of the ridge is built by intrusion, not extrusion. A reasonable estimate of the amount of partial melting which is required to produce alkali basalts is 0·10 (Sun & Hanson, 1975), with tholeiites requiring perhaps 0·2 (Jaques & Green, 1980, see Fig. 10*b*). If therefore the melt fraction required beneath Hawaii is 0·15,

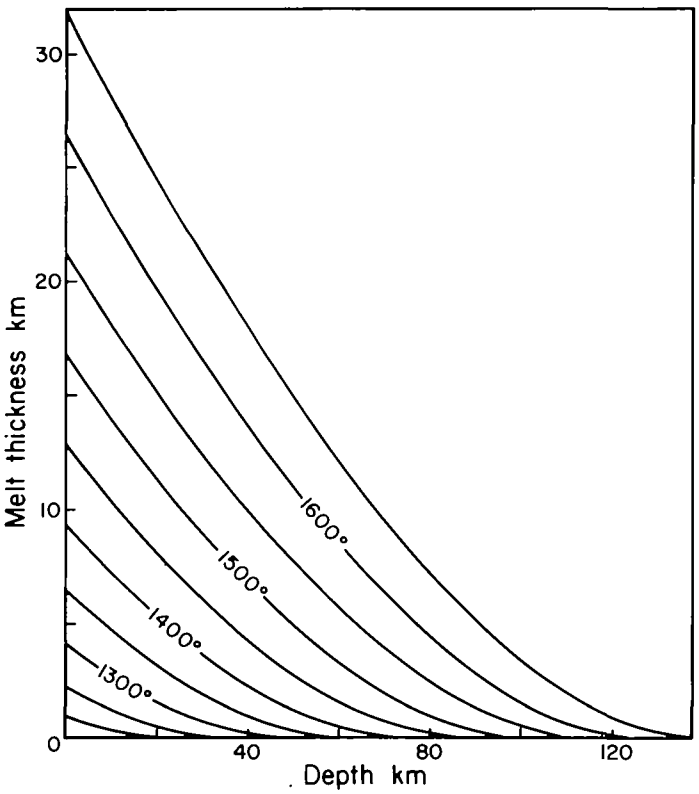

FIG. 12. (continued)

about $1{\cdot}3 \times 10^9$ m^3 yr^{-1} of mantle material must pass through the melting zone. If the upwelling rate is 30 mm yr^{-1} and the jet has a circular cross section, its radius must be about 120 km. The thickness of the vertical part of the jets observed in two dimensional numerical calculations is about 100–150 km (see McKenzie *et al.*, 1980). There is therefore no obvious difficulty in generating the observed quantities of melt in this way. The required fraction of partial melt should be present at a depth of about 70 km if all the melt can be extracted.

An obvious feature of the geotherms in Fig. 12*b* is that the temperature differences within the zone in which partial melting occurs are smaller than those in the solid part of the mantle, because melting acts as a buffer on the temperature. Therefore the temperature difference of about 200 °C between the hot rising jet and the surrounding mantle is reduced to 70 °C by partial melting, with presumably a corresponding reduction in the conductive heat flux. If the melt is removed, as it is beneath Hawaii, the latent heat will be released in the vulcanism, and not in the mantle.

This discussion has shown that the magnitude of the likely variations in temperature produced by the convective circulation can account for the known major volcanic features in some detail. This success suggests that Fig. 12 can be applied to problems about which less is known, such as continental vulcanism within plate interiors and sedimentary basins. Cox (1980) has argued that the extensive tholeiitic plateau basalts are produced by differentiation of a picritic magma. If such basalts are the surface expression of a hot rising jet, then Fig. 12*c* shows that the quantity of magma required can easily be generated.

The other situation in which major quantities of melt are sometimes, but not always,

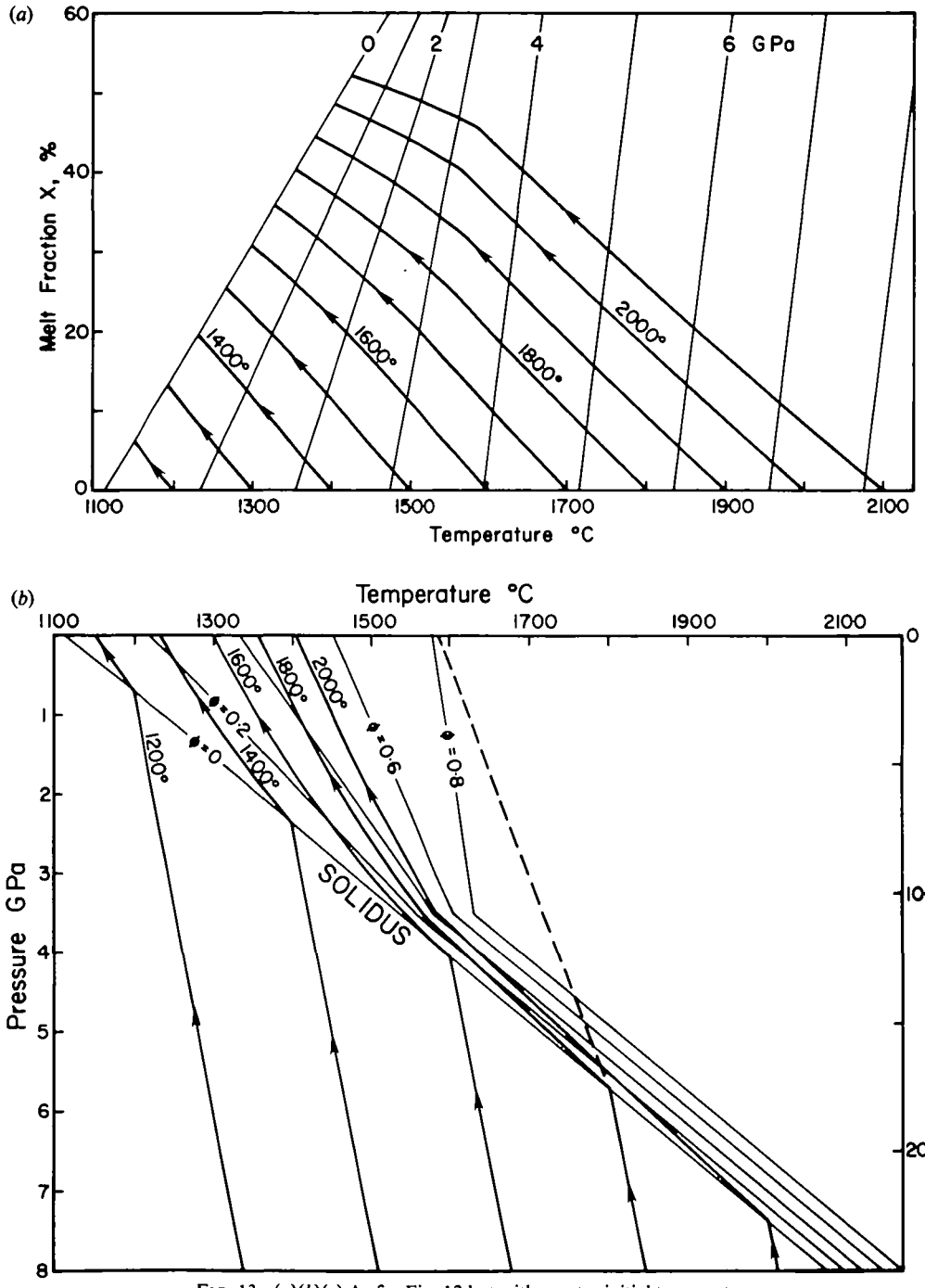

FIG. 13. (*a*)(*b*)(*c*) As for Fig. 12 but with greater initial temperatures.

produced is during the extension of continental crust to produce sedimentary basins. Fig. 12 can be used to estimate the thickness of the volcanic layer which can be produced in this way. If, for instance the lithosphere is stretched by a factor of 3, its base will be at a depth of about 40 km after the stretching event if it is instantaneous. Fig. 12*c* shows that such thinning could

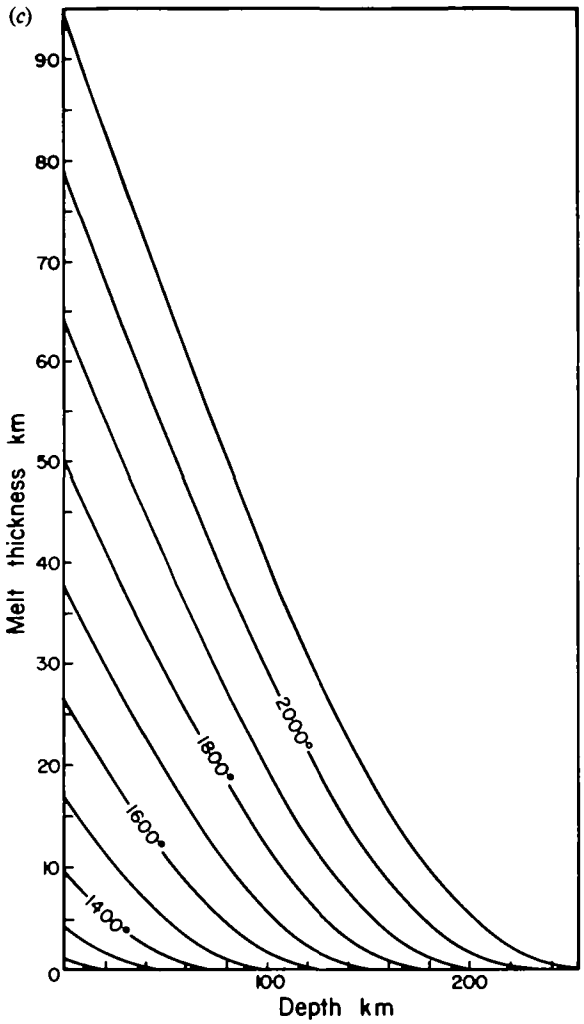

FIG. 13. (continued)

produce as much as 10 km of melt if the stretched region was above a rising jet. But smaller amounts of extension above mantle whose temperature is that of the mean should give rise to little or no vulcanism. These results are therefore compatible with McKenzie's (1984) suggestion that substantial additions to the volume of the continental crust sometimes occur during extension.

Fig. 7*b* also illustrates the importance of the adiabatic decompression of the melt. The resulting change in temperature depends on the depth at which the melt and matrix separate, and is likely to be as large as 100 °C for magma such as those in Hawaii which have separated below the plate.

The agreement between the calculated melt volumes and those observed is encouraging, and suggests that these simple calculations are sufficient to understand the main features of magma generation beneath ridge axes and intraplate volcanoes. In contrast, beneath island arcs the temperature, composition and volatile content are all too poorly known for such calculations to be carried out. It is, however, possible to use the same model to investigate the

conditions required for the generation of komatiites by isentropic melting. Komatiites were generated during the Archaean, when the mean temperature of the mantle was probably between 200 and 300 °C hotter than at present, or 1550–1650 °C. Because the mean viscosity of the mantle must have been considerably smaller than it is now, the excess temperature of the hot rising jets was probably less than at present, perhaps 100 °C. Isentropic upwelling paths in Fig. 13 show that these initial conditions could produce melt fractions of up to about 40 per cent, with eruption temperatures of less than 1400 °C. Such paths would produce enormous volumes of melt (Fig. 13*c*). The problem with such an origin for komatiites is that the magma temperatures at the surface must have been nearer 1600 °C for those containing more than 30 per cent MgO (Nisbet, 1982), and melt fractions of greater than 40 per cent are suggested by some interpretations of the trace element data (Sun & Nesbitt, 1977, 1978), and by laboratory experiments (Fig. 10*b*). Fig. 13*b* shows no isentropic paths which satisfy both these constraints, because the temperature is buffered by melting. Such an origin for komatiites therefore seems improbable, especially since they are relatively uncommon even in the Archaean. The enormous volumes which isentropic melting would produce would dominate exposures of Archaean rock. An alternative origin for magmas whose surface temperature is 1600 °C is to generate them at considerable depths, where they separate from the matrix and upwell isentropically. Such a path is shown in Fig. 13*b*, and would require the magma to be generated at a depth of about 150 km by melting relatively small amounts of the rock. This proposal is similar to that made by O'Hara *et al.* (1975). They also argued that such origin is consistent with the melting relationships observed in garnet peridotites. At high pressures small melt fractions contain a greater percentage of MgO than do those at low pressure. The only important objection to such a proposal is the rare earth abundances (Sun & Nesbitt, 1977, 1978). However, all arguments which depend on such observations depend on assumptions about the composition of the rock undergoing partial melting and about the distribution coefficients between melt and matrix at high pressures. Neither is well determined.

Melt extraction

The arguments in sections 2 and 3 and in Appendices A and B show that melt extraction from partially molten material is always controlled by the rate of deformation of the matrix, and may or may not also be governed by the permeability of the matrix and the viscosity of the melt. The solutions shown in Figs. 1–3 illustrate the type of behaviour which can occur in compacting regions. The magnitude of the fluidization velocity w_0, the compaction length δ_c and the compaction time scale τ_0 have been calculated for two relationships between permeability and porosity (see section 4). These calculations use the values of the quantities given in Table 1, several of which are uncertain. But they do illustrate some important features of the flow. The fluidization velocity is likely to exceed 10 mm yr^{-1} for values of $\phi > 0{\cdot}03$. Hence equilibrium melting is likely to be restricted to small melt fractions. Even the generation of nephelinites by between 3 and 7 per cent melting (Sun & Hanson, 1975) will involve relative movement between the melt and matrix. Such a result is scarcely surprising if nephelinite magmas are primary, since they must then be capable of separating from the matrix.

The velocity with which a melt can move also governs its ability to escape from the convecting region. In hot rising regions the velocities are probably between 10 and 30 mm yr^{-1}, and the melt must be able to move with a comparable velocity if it is to escape. Fig. 14*a* shows that the limiting melt fraction obtained in this way is about 3 per cent. This value was therefore used in Fig. 7 as an upper bound on the fraction of melt likely to be retained by the matrix. For melt fractions as large as 10 per cent the fluidization velocity reaches 1 m yr^{-1}. Separation of melt and matrix will be rapid, and it is unlikely that such large melt fractions are

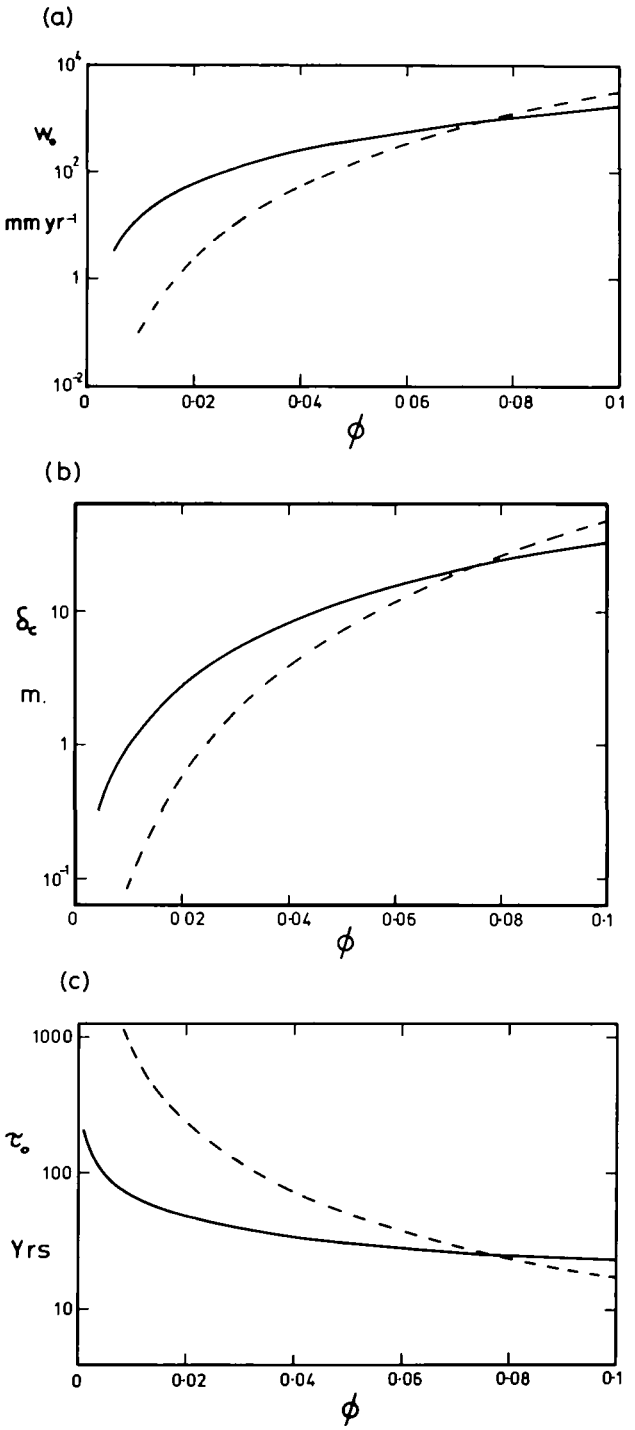

FIG. 14. (*a*) The minimum fluidization velocity w_0 as a function of porosity ϕ, obtained from (3.7) and the values of the constants in Table 1, for (4.3), shown as a dashed, and (4.4), shown as a solid, line. (*b*) The compaction length δ_c as a function of the porosity ϕ, obtained from (3.3) and the values of the constants in Table 1, for (4.3), shown as a dashed, and (4.4), shown as a solid, line. (*c*) The time scale for compaction τ_0 as a function of the porosity ϕ, obtained from (B11) and the values of the constants in Table 1, for (4.3) shown as a dashed, and (4.4), shown as a solid, line.

ever present within the earth. The same result is expected from Fig. 14*c* which shows that the compaction occurs rapidly even when the amount of partial melt is as small as 1 per cent. These arguments suggest that, of the various melting models commonly discussed by igneous petrologists (see Cox *et al.*, 1979), Rayleigh melting should most closely resemble the behaviour of melts in the mantle. Such a model will not, however, provide a useful method of estimating the magma composition because of the motion relative to the matrix.

The results provide an explanation of the seismic and gravity interpretations of ridge axes. Fowler (1976) shot several seismic lines parallel to and across the Mid-Atlantic Ridge axis, and found that shear waves propagated everywhere. Lewis & Garmany (1982) failed to find an extensive low velocity region beneath the East Pacific Rise. There therefore is little evidence for extensive regions containing a large amount of partially molten material. Another important result is that Lewis (1982) required a narrow region about 5 km across of density 3·1 Mg m^{-3} beneath the axis of the East Pacific Rise. This region must extend to within about 4 km of the sea floor, and be 0·5 Mg m^{-3} denser than the oceanic crust. These properties are consistent with the presence of partially molten mantle with no more than a few per cent of the melt beneath the ridge axis, from which the normal thickness of oceanic crust is generated by compaction.

The other result of interest is the magnitude of the compaction length, which is unlikely to exceed 100 m. Therefore thin sheets of partially molten material should be able to compact. This result, combined with the short compaction time scale in Fig. 14*c*, suggests that useful estimates of the matrix viscosities can be made from the porosity distribution in differentiating sills if the crystalline material formed from the melt can be distinguished from the matrix.

The time scales and velocities in Fig. 14 show that movement between melt and matrix will be a general feature of partially molten regions within the earth. Ahern & Turcotte (1978) also recognized that relative movement between melt and matrix would occur and attempted to include this effect in their calculations. They did not, however, realize that the compaction rate is controlled by the rate of deformation of the matrix, and their calculations should therefore be repeated using the equations derived in Appendix A.

The estimates of the compaction length and compaction time scale in Fig. 14 depend on the square root of the viscosities of the matrix. Though they should be recalculated when more reliable values are available for ζ and η, the arguments above are not likely to be affected.

Thermal and geochemical variations

Frank (1968) and Felgett (written communication, 1982) have considered the possibility of thermal convection in the melt phase alone. Such flow will only be important if the Rayleigh number appropriate to convection in a porous medium, defined by (3.9), exceeds $4\pi^2$. The quantities in Table 1 can be used to estimate h, the required depth of the layer, if ϕ and the difference between the temperature gradient and the adiabatic temperature gradient are known. Taking $\phi = 0{\cdot}1$ and the difference in the gradients as 1 °C/km yields a value of h of 100 km if the upper of the two curves relating the permeability and porosity is used. Since the fluidization velocity of $\phi = 0{\cdot}1$ is more than 1 m yr^{-1}, the melt will not remain dispersed. It is therefore not likely that thermal convection within the melt alone occurs.

A more important effect is the variation of the effective transport velocity between different elements. The ratio of the effective velocity w_e to the melt velocity w is derived in Appendix E

$$w_e/w = \left[\left(\frac{1}{\phi} - 1\right)\frac{\rho_s}{\rho_f}K_c + 1\right]^{-1} \tag{5.3}$$

where K_c is the distribution coefficient (by weight) between the solid and the melt. This

equation is only valid if the melt is in equilibrium with the matrix, and the necessary conditions which must be satisfied are examined in Appendix E. Equation (5.3), which applies to trace elements, and in a modified form to major elements also, is at first sight wrong, since it predicts that the major elements of which the melt consists will not travel with the melt velocity. This intuitive objection is, however, incorrect because of the exchange which takes place between the matrix and melt. Because only that fraction of the element which is in the melt is in motion, the effective transport velocity is less than the melt velocity, because the melt must transport the element present in both solid and liquid phases. This velocity can only be determined by measuring the movement of a change in concentration or by using an isotopic tracer. Hence variations in the transport rate will only be important where variations in the concentration of some element in the melt occur. Such variation can be produced either by initial variations in the source rock or by differences in the amounts of partial melting in an initially uniform rock.

It is straightforward to apply (5.3) to trace element transport, since the variation of the activity coefficient with concentration can be ignored. For this reason only such elements are discussed here. In the case of major elements the distribution coefficient in (5.3) must be replaced by the concentration ratio c_s/c_l, which is not in general independent of the concentrations. The equation governing the transport is then no longer linear. Jacobsen & Wasserburg (1979) and Pearce & Norry (1979) list values of K_c for a number of trace elements between clinopyroxene and melt, and between olivine and melt. These values have been used to calculate the effective velocities as functions of the melt fraction of clinopyroxene and olivine (Fig. 15*a* and *b*). If the matrix consists of olivine alone, the ratio (5.3) is little different from 1 for K, Rb, Sr and U for probable values of ϕ. The two rare earths, however, travel significantly more slowly than the mean melt velocity. A clinopyroxene matrix has a much greater influence, and Nd and Sm travel with only about 1/10th the velocity of the melt when $\phi = 0{\cdot}03$. This behaviour is illustrated in another way in Fig. 16, where the melt porosity is

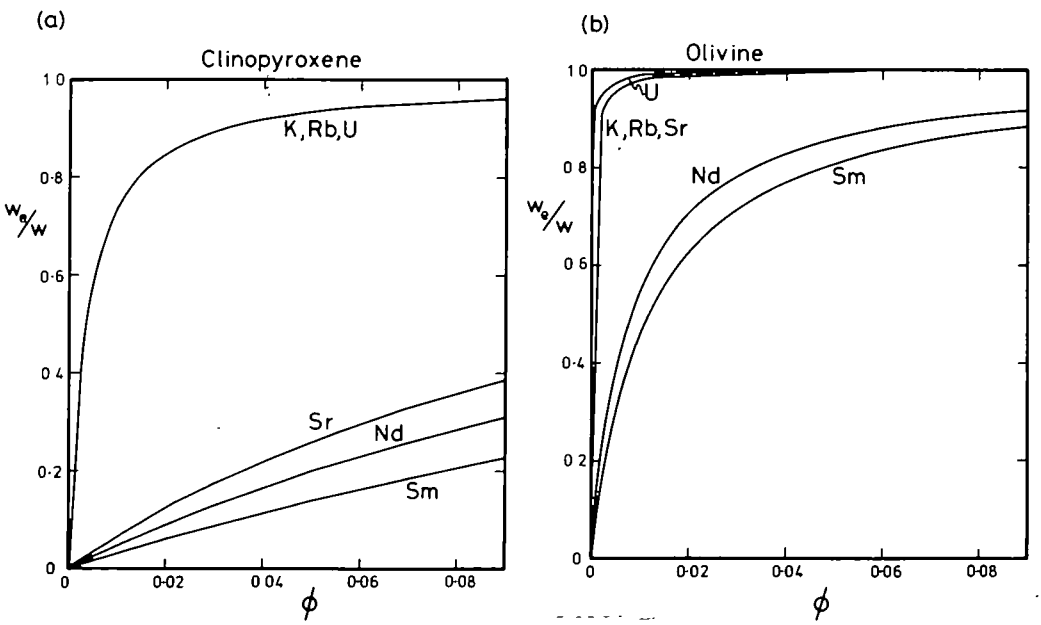

FIG. 15. The ratio of the transport velocity, w_e to the mean velocity w for six elements, calculated using (5.3) and the distribution coefficients given by Jacobsen & Wasserburg (1979), when the matrix consists of clinopyroxene, (*a*), and olivine, (*b*).

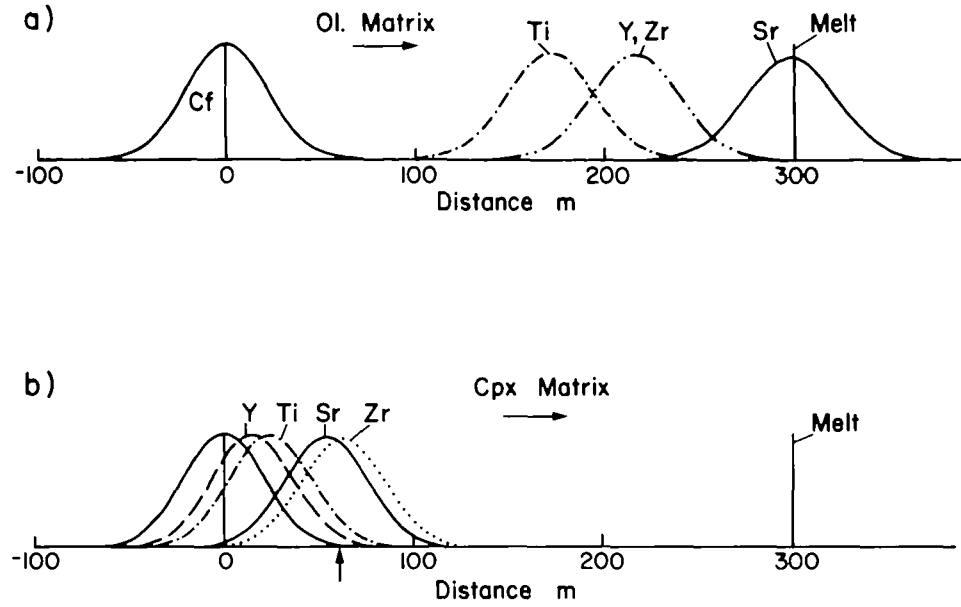

FIG. 16. The initial concentration of all four trace elements has a gaussian distribution about the origin, with $c_f(0) = 1$ and falling to 1/e at ± 30 m. The elements are transported to the right by the movement of melt in the direction of the arrow. The porosity is 3 per cent. The concentration profiles marked Ti, Y, Zr and Sr show the movement of these elements produced by the movement of the melt from the origin to the position of the line at the right, obtained using (E24) and the distribution coefficients given by Pearce & Norry (1979). The length of the line marked 'melt' is unity, and the decrease in height of the curve marked Sr in (*a*) results from dispersion. (*a*) Shows the effect of an olivine matrix, (*b*) that of clinopyroxene. The arrow below the axis in (*b*) shows the position at which the concentrations in Fig. 17 are calculated.

assumed to be 3 per cent everywhere. A gaussian variation in concentration of Ti, Y, Zr and Sr with a width of 60 m is introduced, centred on the origin. As the melt moves uniformly towards the right with velocity w it carries the trace elements with it. The centres of the concentration anomalies move with velocities w_e, and, especially when the matrix contains clinopyroxene, $w_e \ll w$. The effect is important even when the matrix consists of olivine. Clearly such behaviour depends on variations in concentrations within the melt. These are likely to be widespread, due to variations in the degree of partial melting. Fig. 16 also shows that the concentration anomalies are spread out by the melt movement. The initial concentration is unity, and is reduced by the transport as the width of the gaussian curve increases. This effect is easily visible for Sr in an olivine matrix, and is called dispersion.

The transport of trace elements through a matrix at different velocities can also be illustrated with a triangular diagram of the type used by Pearce & Cann (1973) to classify basic volcanic rocks by their tectonic setting. Fig. 17 shows a diagram for a point 60 m to the right of the origin in Fig. 16*b* as the trace elements are carried past. Zr travels most rapidly, and therefore its concentration at first increases relative to that of Ti and Y. As the Zr peak passes Ti arrives and finally Y. The magnitude of the variations are quite sufficient to account for those observed by Pearce & Cann (1973).

The behaviour illustrated in Figs. 15 to 17 suggests that trace element concentrations may provide a means of studying the relative movement between melt and matrix as they separate. Though the isotopic ratios will not themselves be affected, the strontium and neodymium ratios measured in a glass will not necessarily be related to each other in the same way as they were in the source rock, because the two elements travel with different velocities.

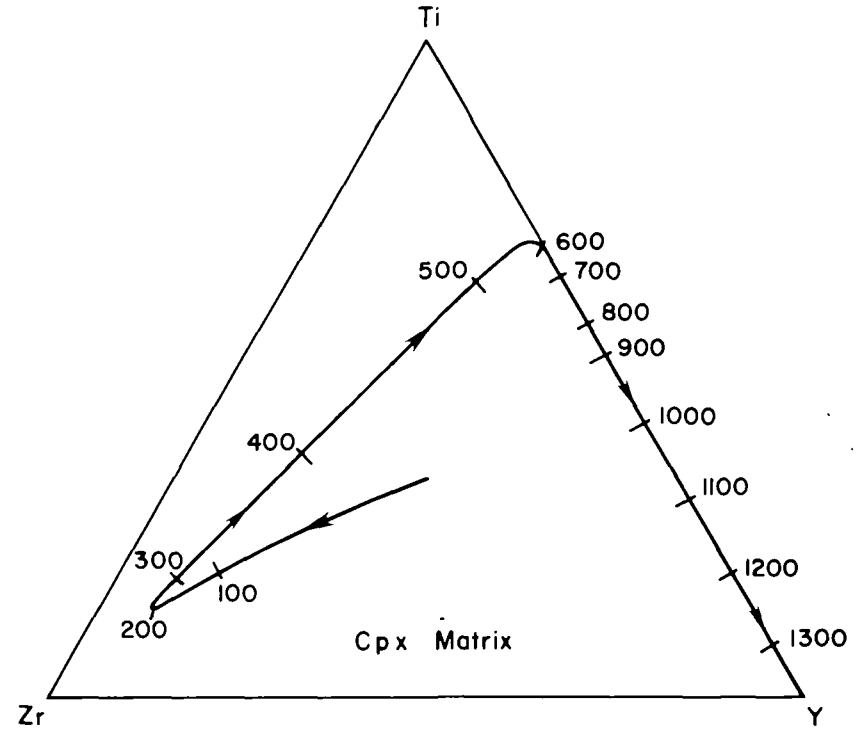

FIG. 17. A ternary diagram, of the type used by Pearce & Cann (1973) to classify basic igneous rocks, but showing the variation in concentration of the three elements at a point 60 m to the right of the origin in 16(*b*) as a function of the distance travelled by the melt, marked on the curve in metres.

Nor need the concentration of the parent elements Rb and Sm in the glass be related to that of their decay products. How important these effects may be can most easily be determined by numerical calculations.

The other problem of geochemical interest is the effect of partial melting in the asthenosphere on the scale of mantle heterogeneities. In the solid part of the mantle the bulk diffusivity limits the inhomogeneities to scales greater than a few tenths of a metre. If the material spends 20 Myr in a partially molten region, diffusion in the melt will increase the minimum scale of variations to at least 20 m, even if no relative motion occurs between the melt and matrix.

The final question concerns the variation of dispersion with the melt velocity. If the percolation velocity is sufficiently rapid, the dispersion is purely geometric. It is independent of the percolating velocity and depends only on the distance travelled. The condition which must be satisfied before this type of behaviour occurs is given by (E25), which requires

$$|\mathbf{v}| \gg 3 \text{ m yr}^{-1}$$

This condition is not likely to be satisfied in most compacting regions.

6. CONCLUSIONS

The most important part of this paper is contained in Appendix A, where the equations governing the motion of the melt and matrix are obtained. Simple solutions demonstrate that the compaction of a partially molten material is always controlled by the properties of the

matrix, and generally by those of the melt as well. Two parameters, the shear and the bulk viscosity, govern the rate of deformation of the matrix, and neither can yet be estimated with any accuracy. A number of simple laboratory experiments are proposed which could yield estimates of these quantities and their variation with porosity. It is also likely that useful estimates can be obtained from the petrography of cooling sills in which differentiation has occurred. In all cases it is important to establish that the pore geometry is in equilibrium. The viscosities and permeability of the matrix will depend on the porosity and grain size, which should both be measured. In addition they will depend on the pore geometry, which is largely controlled by the dihedral angle. It is particularly important that this angle should also be measured.

A simple model can be used to investigate the variation of melt fraction with depth during upwelling at constant entropy if the melt and solid are not in relative motion. Though the melt must move relative to the matrix if magma is to be erupted, the effect of this motion can be estimated and is comparable to the uncertainty in the latent heat of melting. The model illustrates how the geotherm is controlled by the amount of partial melting, rather than vice versa as is often assumed in the geological literature.

The isentropic upwelling model permits the melt fraction to be calculated directly as a function of depth. Material upwelling with an initial temperature of 1350 °C meets the solidus at a depth of about 60 km, and the melt fraction reaches 20 per cent at the surface. The total amount of melt generated is sufficient to produce the oceanic crustal thickness if it is all extracted. These conclusions principally depend on the latent heat of melting, laboratory measurements of the solidus as a function of pressure, and on the density contrast between matrix and melt. They only depend weakly on the form assumed for the variation of melt fraction with pressure and temperature. When ridge axes are above hot rising jets in the mantle, the initial temperature is likely to be about 1550 °C. Such material can produce a crustal thickness of more than 20 km, with more than 35 per cent of the material melting near the surface. If such a jet lies beneath a plate interior, sufficient melting can occur to generate the Hawaiian Ridge if about 15 per cent of the upwelling material is melted. All these estimates are in satisfactory agreement with, and are independent of, petrological and geochemical estimates. The same model can be used to investigate the origin of komatiites, and shows that it is unlikely that these magmas originate near the surface. They may, however, be produced at depths of about 150 km or more by relatively small (~20 per cent) amounts of partial melting, in agreement with the suggestions of O'Hara *et al.* (1975).

The isentropic upwelling model is only useful if the quantity of magma left in the matrix can be estimated. Estimates of the relative velocity between melt and matrix and of the compaction time scale suggest that melt and matrix will separate rapidly in upwelling regions. The melt fraction is therefore unlikely to exceed a few per cent anywhere at a particular time within the mantle, and less than 3 per cent is likely to remain within the matrix. Since the fraction which melts probably exceeds 30 per cent, equilibrium melting (where there is no relative velocity between the melt and matrix) is likely to be uncommon. Rayleigh melting should be a better model, but, because of the relative movement between melt and matrix, cannot be used to calculate the melt composition.

Movement between melt and matrix can also have important geochemical effects on the trace element distributions. If an appreciable fraction of an element remains within the matrix, its transport velocity is less than the melt velocity. The matrix then behaves in the same way as a separation column. The magnitude of the effect depends on the distribution coefficient. Those for K, Rb, Sr, U, Nd and Sm show that an olivine matrix has little effect on the transport velocities of the first four of these elements. In the case of the rare earths, however, the velocity is only about 70 per cent of the melt velocity when the porosity is 3 per cent. If,

however, the matrix consists of clinopyroxene the effect is considerably larger, and Sm travels with only 10 per cent of the melt velocity. This effect may be geochemically important, especially if clinopyroxene is present. It may be possible to use trace element distributions to investigate the separation of melt from matrix.

ACKNOWLEDGEMENTS

The ideas in this paper have been clarified by many useful conversations with F. Richter. I would also like to thank S. Agrell, M. Bickle, M. Bowie, K. Cox, C. Donaldson, P. England, G. Fitton, R. Kerr, S. Maaløe, M. Nevitt, M. O'Hara, R. Poeppel, M. Ryan, D. Walker and N. Zaichick for their help and suggestions. This work was supported by the National Science Foundation at Harvard University by grant EAR81-09464 and at the University of Chicago by EAR82-00003, and by NERC at Cambridge by GR3/5607.

REFERENCES

Ahern, J. L., & Turcotte, D. L., 1979. Magma migration beneath an ocean ridge. *Earth planet. Sci. Lett.* **45**, 115–22.

Artz, E., Ashby, M. F., & Easterling, K. E., 1983. Practical applications of hot-isostatic pressing diagrams. *Metallurgical Trans.* **14A**, 211–21.

Anderson, T. B., & Jackson, R., 1968. Fluid mechanical description of fluidized beds: stability of state of uniform fluidization. *Indust. Engineer. Chem. Fundamentals*, **7**, 12–21.

—— —— 1969. A fluid mechanical description of fluidized beds. Comparison of theory and experiment. *Ibid.* **8**, 137–44.

Batchelor, G. K., 1967. *An Introduction to Fluid Dynamics*. Cambridge University Press.

Bear, J., 1972. *Dynamics of Fluids in Porous Media*. New York: American Elsevier.

Beeré, W., 1975*a* A unifying theory of the stability of penetrating liquid phases and sintering pores. *Acta Metall.* **23**, 131–8.

—— 1975*b*. The second stage sintering kinetics of powder compacts. *Ibid.* **23**, 139–45.

—— 1981. The internal morphology of continuously interconnected two phase bodies. *Trans. J. Br. Ceram. Soc.* **80**, 133–8.

Berckhemer, H., Baier, B., Bartelson, H., Behle, A., Burkhardt, H., Gebrande, H., Makris, J., Menzel, H., Miller, H., & Vees, R., 1975. Deep seismic soundings in the Afar region and on the highland of Ethiopia. In: Pilger, A., & Rosler, A. (eds.) *Afar Depression of Ethiopia*. Stuttgart: E. Schweizerbart'sche Verlagsbuchhandlung, 89–107.

Bott, M. H. P., & Gunnarsson, K., 1980. Crustal structure of the Iceland–Faeroe Ridge. *J. Geophys.* **47**, 221–7.

Bowen, L. J., Weston, R. J., Carruthers, T. G., & Brook, R. J., 1976. Mechanisms of densification during the pressure sintering of alpha-silicon nitride. In: Vincenzini, P. (ed.) *Proc. 3rd CIMTEC Conference, Advances in Ceramic Processing*, 162–5.

Budiansky, B., 1970. Thermal and thermoelastic properties of isotropic composites. *J. Composite Materials*, **4**, 286–95.

Bulau, J. R., Waff, H. S., & Tyburczy, J. A., 1979. Mechanical and thermodynamic constraints on fluid distribution in partial melts. *J. geophys. Res.* **84**, 6102–8.

Cox, K. G., 1980. A model for flood basalt vulcanism. *J. Petrology*, **21**, 629–50.

—— Bell, J. D., & Pankhurst, R. J., 1979. *The Interpretation of Igneous Rocks*. London: George Allen & Unwin.

Crittenden, M. D., 1963. Effective viscosity of the earth derived from isostatic loading of Pleistocene Lake Bonneville. *J. geophys. Res.* **68**, 5517–30.

Dane, E. D., 1941. Densities of molten rocks and minerals. *Am. J. Sci.* **239**, 809–18.

Didwania, A. K., & Homsy, G. M., 1981. Flow regimes and flow transitions in liquid fluidized beds. *Int. J. Multiphase Flow*, **7**, 563–80.

—— —— 1982. Resonant sideband instabilities in wave propagation in fluidized beds. *J. Fluid Mech.* **122**, 433–8.

Drew, D. A., 1971. Averaged field equations for two-phase media. *Stud. Appl. Maths.* **50**, 133–66.

—— 1983. Mathematical modelling of two-phase flow. *Ann. Rev. Fluid Mech.* **15**, 261–91.

—— & Segel, L. A., 1971. Averaged equations for two-phase flows. *Stud. Appl. Maths.* **50**, 205–31.

Dullien, F. A. L., 1979. *Porous Media Fluid Transport and Pore Structure*. New York: Academic Press.

Durney, D. W. 1976. Pressure-solution and crystallization deformation. *Phil. Trans. R. Soc. Lond.* **A283**, 229–40.

El-Kaissy, M. M., & Homsy, G. M., 1976. Instability waves and the origin of bubbles in fluidized beds. I. Experiments. *Int. J. Multiphase Flow*, **2**, 379–95.

Elliot, D., 1973. Diffusion flow laws in metamorphic rocks. *Bull. geol. Soc. Am.* **84**, 2645–64.

Fowler, C. M. R., 1976. Crustal structure of the Mid-Atlantic ridge crest at 37° N. *Geophys. J.R. astr. Soc.* **47**, 459–91.

Frank, F. C., 1968. Two-component flow model for convection in the Earth's upper mantle. *Nature*, **220**, 350–2.
Gessinger, G. H., & Fischmeister, H. F., 1972. A modified model for the sintering of tungsten with nickel additions. *J. Less Common Metals*, **27**, 129–41.
Goslin, J., Recq, M., & Schlich, R., 1981. Structure profonde du Plateau de Madagascar: relations avec le Plateau de Crozet. *Tectonophys.* **76**, 75–97.
Hashin, Z., 1964. Theory of mechanical behaviour of heterogeneous media. *Appl. Mech. Rev.* **17**, 1–9.
Herzberg, C. T., 1983. Solidus and liquidus temperatures and mineralogies for anhydrous garnet-lhernolite to 15 GPa. *Phys. Earth planet. Inter.* **32**, 193–202.
Hofmann, A. W., & Hart, S. R., 1978. An assessment of local and regional isotopic equilibrium in the mantle. *Earth planet. Sci. Lett.* **38**, 44–62.
—— & Margaritz, M., 1977. Diffusion of Ca, Sr, Ba and Co in a basalt melt: implications for the geochemistry of the mantle. *J. geophys. Res.* **82**, 5432–40.
Homsy, G. M., El-Kaissy, M. M., & Didwania, A. K., 1980. Instability waves and the origin of bubbles in fluidized beds. II. Comparison with theory. *Int. J. Multiphase Flow*, **6**, 305–18.
Houseman, G., 1983. The deep structure of ocean ridges in a convecting mantle. *Earth planet. Sci. Lett.* **64**, 283–94.
—— & McKenzie, D. P., 1982. Numerical experiments on the onset of convective instability in the earth's mantle. *Geophys. J.R. astr. Soc.* **68**, 133–64.
Jacobson, S. B., & Wasserberg, G. T., 1979. The mean age of mantle and crustal reservoirs. *J. geophys. Res.* **84**, 7411–27.
Jaques, A. L., & Green, D. H., 1980. Anhydrous melting of peridotite at 0–15 kb pressure and the genesis of tholeiitic basalts. *Contr. Miner. Petrol.* **73**, 287–310.
Kamb, B., 1972. Experimental recrystallization of ice under stress. In: Heard, H. C. *et al.* (eds.) *Flow and Fracture in Rocks. Am. geophys. Union Monograph*, **16**, 211–41.
Landau, L. D., & Lifshitz, E. M., 1959. *Fluid Mechanics*. London: Pergamon Press.
Lewis, B. T. R., 1982. Constraints on the structure of the East Pacific Rise from gravity. *J. geophys. Res.* **87**, 8491–500.
—— & Garmany, J. D., 1982. Constraints on the structure of the East Pacific Rise from seismic refraction data. *Ibid.* **87**, 8417–25.
Liu, J. T. C., 1982. Note on a wave-hierarchy interpretation of fluidized bed instabilities. *Proc. R. Soc. Lond.* **A380**, 229–39.
Maaløe, S., & Printzlau, I., 1979. Natural partial melting of spinel lherzolites. *J. Petrology*, **20**, 727–41.
—— & Scheie, A., 1982. The permeability controlled accumulation of primary magma. *Contr. Miner. Petrol.* **81**, 350–7.
McKenzie, D. P., 1984. A possible mechanism for epeirogenic uplift. *Nature*, **307**, 616–8.
—— Watts, A., Parsons, B., & Roufosse, M., 1980. Planform of mantle convection beneath the Pacific Ocean. *Nature*, **288**, 442–6.
Minster, J. B., & Jordan, T. H., 1978. Present-day plate motions. *J. geophys. Res.* **83**, 5331–54.
Miyamoto, M., & Takeda, H., 1983. Atomic diffusion coefficients calculated for transition metals in olivine. *Nature*, **303**, 602–3.
Murase, T., & McBirney, A. R., 1973. Properties of some common igneous rocks and their melts at high temperatures. *Bull. geol. Soc. Am.* **84**, 3563–92.
Mysen, B. O., & Kushiro, I., 1977. Compositional variations of coexisting phases with degree of melting of peridotite in the upper mantle. *Am. Miner.* **62**, 843–65.
Nisbet, E. G., 1982. The tectonic setting and petrogenesis of komatiites. In: Arndt, N. T. & Nisbet, E. G. (eds.) *Komatiites*. London: George Allen & Unwin, 501–20.
O'Hara, M. J., Saunders, M. J., & Mercy, E. L. P., 1975. Garnet-peridotite, primary ultrabasic magma and eclogite; interpretation of upper mantle processes in kimberlite. *Phys. Chem. Earth*, **9**, 571–604.
Parsons, B., & McKenzie, D. P., 1978. Mantle convection and the thermal structure of plates. *J. geophys. Res.* **83**, 4485–96.
—— & Sclater, J. G., 1977. An analysis of the variation of ocean floor bathymetry and heat flow with age. *Ibid.* **82**, 803–27.
Pearce, J. A., & Cann, J. R., 1973. Tectonic setting of basic volcanic rocks determined using trace element analyses. *Earth planet. Sci. Lett.* **19**, 290–300.
—— & Norry, M. J., 1979. Petrogenetic implications of Ti, Zr, Y, and Nb variations in volcanic rocks. *Contr. Miner. Petrol.* **69**, 33–47.
Pharr, G. M., & Ashby, M. F., 1983. On creep enhanced by a liquid phase. *Acta Metall.* **31**, 129–38.
Podob, M. T., 1977. Effect of heat treatment and slight chemistry variations on the physical metallurgy of hot isostatically pressed low carbon astrology powder. *Modern Developments in Power Metall.* **11**, 25–44.
Raj, R., & Chyung, C. K., 1981. Solution–precipitation creep in glass ceramics. *Acta Metall.* **29**, 159–66.
Richter, F. M., & McKenzie, D. P., 1978. Simple plate models of mantle convection. *J. Geophys.* **44**, 441–71.
Ruegg, J. C., 1975. Main results about the crustal and upper mantle structure of the Djibouti region (T.F.A.I.). In: Pilger, A., & Rosler, A. (eds.) *Afar Depression of Ethiopia*. Stuttgart: E. Schweizerbart'sche Verlagsbuchhandlung, 120–34.
Rumpf, H., & Gupte, A. R., 1971. Einflusse der Porositat und Korngrossenverteilung im Widerstandsgesetz der Porenstromung. *Chemie-Ing. Techn.* **43**, 367–75.

Rutter, E. H., 1976. The kinetics of rock deformation by pressure solution. *Phil. Trans. R. Soc. Lond.* **A283**, 203–19.
Saffman, P. G., & Taylor, G. I., 1958. The penetration of a fluid into a porous medium or Hele-Shaw cell containing a more viscous liquid. *Proc. R. Soc. Lond.* **A245**, 312–29.
Sinha, M. C., Louden, K. E., & Parsons, B., 1981. The crustal structure of the Madagascar Ridge. *Geophys. J.R. astr. Soc.* **66**, 351–77.
Sleep, N. H., 1969. Sensitivity of heat flow and gravity to the mechanism of sea-floor spreading. *J. geophys. Res.* **74**, 542–9.
—— 1974. Segregation of a magma from a mostly crystalline mush. *Bull. geol. Soc. Am.* **85**, 1225–32.
Stolper, E., Walker, D., Hager, B. H., & Hays, J. F., 1981. Melt segregation from partially molten source regions: the importance of melt density and source region size. *J. geophys. Res.* **86**, 6261–71.
Sun, S. S., & Hanson, G. N., 1975. Origin of Ross Island basanitoids and limitations upon the heterogeneity of mantle sources for alkali basalts and nephelinites. *Contr. Miner. Petrol.* **52**, 77–106.
—— & Nesbitt, R. W., 1977. Chemical heterogeneity of the Archaean mantle, composition of the earth and mantle evolution. *Earth planet. Sci. Lett.* **35**, 429–48.
—— —— 1978. Petrogenesis of Archaean ultrabasic and basic volcanics: evidence from rare earth elements. *Contr. Miner. Petrol.* **65**, 301–25.
Takahashi, E., & Kushiro, I., 1983. Melting of a dry peridotite at high pressures and basalt magma genesis. *Am. Miner.* **68**, 859–79.
Taylor, G. I., 1954. The two coefficients of viscosity for an incompressible fluid containing air bubbles. *Proc. R. Soc. Lond.* **A226**, 34–9.
Vaughan, P. J., & Kohlsted, D. L., 1982. Distribution of the glass phase in hot-pressed olivine basalt aggregates: an electron microscopy study. *Contr. Miner. Petrol.* **81**, 253–61.
Verhoogen, J., 1965. Phase changes and convection in the earth's mantle. *Phil. Trans. R. Soc. Lond.* **A258**, 276–83.
Verrall, R. A., & O'Connell, R. J., 1981. Pressure solution deformation of wet salt. (unpublished manuscript)
Wadge, G., 1980. Output rate of magma from active central volcanoes. *Nature*, **288**, 253–5.
Waff, H. S., 1980. Effects of the gravitational field on liquid distribution in partial melts within the upper mantle. *J. geophys. Res.* **85**, 1815–25.
—— & Bulau, J. R., 1979. Equilibrium fluid distribution in an ultramafic partial melt under hydrostatic stress conditions. *Ibid.* **84**, 6109–14.
Walker, D., Stolper, E. M., & Hays, J. F., 1978. A numerical treatment of melt/solid segregration: size of eucrite parent body and stability of terrestrial low-velocity zone. *J. geophys. Res.* **83**, 6005–13.
Watson, B. E., 1982. Melt infiltration and magma evolution. *Geology*, **10**, 236–40.
Watts, A. B., 1976. Gravity and bathymetry in the central Pacific Ocean. *J. geophys. Res.* **81**, 1533–53.

APPENDIX A

The equations governing two phase flow

There is an extensive literature concerned with the fluid dynamics of mixtures of fluids. The approach taken here is a simplification of that of Drew (1971, 1983) and Drew & Segel (1971), and is similar to that used by Didwania & Homsy (1982) in their treatment of instabilities of a fluidized bed. The equations derived below only apply to regions which are much larger than the individual grains of the matrix, and treat both the melt and matrix as continuous but interacting phases.

The equations required are those governing the conservation of mass, momentum and energy. If ψ is some quantity associated with either the melt or the matrix which is conserved, then the rate of change of ψ within a fixed volume V must be equal to the rate at which ψ is transported across the surface S bounding V. Hence

$$\frac{\mathrm{d}}{\mathrm{d}t}\int_{\mathrm{v}} \psi \,\mathrm{d}V = -\int_{\mathrm{s}} \psi \mathbf{v}.\mathbf{dS} + \int_{\mathrm{v}} S_\psi \,\mathrm{d}V \qquad \text{(A1)}$$

where $\mathbf{v}$ is the velocity of the material which transports ψ and S_ψ is the rate at which ψ is produced/unit volume. If ψ is the mass/unit volume of the melt, then

$$\psi = \rho_{\mathrm{f}}\,\phi$$

where ρ_{f} is the melt density and ϕ the porosity. Substitution into (A1) and use of Gauss's theorem gives

$$\int_{\mathrm{v}} \left(\frac{\partial(\rho_{\mathrm{f}}\phi)}{\partial t} + \nabla.(\rho_{\mathrm{f}}\phi\mathbf{v}) \right) \mathrm{d}V = \int_{\mathrm{v}} \frac{\mathrm{D}_{\mathrm{v}} M}{\mathrm{D}t}\,\mathrm{d}V \qquad \text{(A2)}$$

where $D_v M/Dt$ is the rate at which mass is transferred from the matrix to the melt, measured in a frame fixed to the matrix, and $\mathbf{v}$ is the velocity of the melt. Equation (A2) must be true for any volume V. Hence

$$\frac{\partial(\rho_f \phi)}{\partial t} + \nabla.(\rho_f \phi \mathbf{v}) = \frac{D_v M}{Dt} \tag{A3}$$

Exactly the same argument applied to the matrix leads to

$$\frac{\partial}{\partial t}(\rho_s(1-\phi)) + \nabla.(\rho_s(1-\phi)\mathbf{V}) = -\frac{D_v M}{Dt} \tag{A4}$$

where $\mathbf{V}$ is the matrix velocity.

The two other equations required govern the conservation of momentum. In these the interaction between the melt and the matrix must be included, by using a body force/unit volume $\mathbf{I}$. If $\mathbf{I}$ is the force on the matrix produced by the movement of the melt, the force on the melt by the matrix must be $-\mathbf{I}$ by Newton's third law. If gravity is included and z is taken to be positive upward, conservation of momentum for the matrix requires

$$\frac{d}{dt}\int_v \rho \mathbf{v}\, dV = -\int_v \rho g \mathbf{a}_z\, dV + \int_v \mathbf{I}\, dV + \int_s \boldsymbol{\sigma}^s.\mathbf{dS} - \int \rho \mathbf{v}\mathbf{v}.\mathbf{dS} \tag{A5}$$

where g is the acceleration due to gravity, $\mathbf{a}_z$ is a unit vector in the +z direction and $\boldsymbol{\sigma}^s$ is the stress tensor acting on the matrix. The velocities of both the matrix and the melt in all the problems discussed below are sufficiently small for the rate of advection of momentum by the flow to be neglected in comparison with its rate of diffusion by viscosity. This statement is equivalent to saying that the Reynolds Number

$$Re = \frac{|\mathbf{v}|L}{\nu} \tag{A6}$$

where L is a characteristic length, $|\mathbf{v}|$ a characteristic velocity and ν the kinematic viscosity, is small compared with unity. In the compaction problem the characteristic length for the melt is the grain size, and typical velocities are less than 1 m yr^{-1}. Substitution into (A6) of the values in Table 1 gives $Re \lesssim 10^{-8}$ for the melt and an even smaller value for the matrix. Therefore the momentum is negligible.

The other approximation which can be made is the neglect of the term on the left of (A5), because the rate of change of the momentum is always small. Therefore forces maintaining the movement must be balanced by the resistive forces at all times. Since the stress within the matrix only acts on that part of the surface S which is inside the matrix, $\mathbf{dS}$ should be replaced by $(1-\phi)\,\mathbf{dS}$ (Drew 1971, equation (2.35)). As before $\rho = (1-\phi)\rho_s$, and (A5) requires

$$-(1-\phi)\rho_s g\, \delta_{i3} + I_i + \frac{\partial}{\partial x_j}[(1-\phi)\sigma^s_{ij}] = 0 \tag{A7}$$

where i and j have the values 1 to 3, $\delta_{ij} = 0$, $i \neq j$; $= 1$, $i = j$, and the Einstein summation convention over repeated subscripts is implied. Equation (A7) is therefore three equations. The first shows the force balance in the x_1, or x, direction. Since $\delta_{13} = 0$ the first term is zero, and the last one must be summed over j from 1 to 3 because j is a repeated subscript. Hence the last term in (A7) is

$$\frac{\partial}{\partial x_1}[(1-\phi)\sigma^s_{11}] + \frac{\partial}{\partial x_2}[(1-\phi)\sigma^s_{12}] + \frac{\partial}{\partial x_3}[(1-\phi)\sigma^s_{13}]$$

where x_2 is y and x_3 is z. The stress tensor $\boldsymbol{\sigma}^s$ is symmetric, so $\sigma^s_{IJ} = \sigma^s_{JI}$. The corresponding equation for the melt is obtained in exactly the same way

$$-\phi\rho_f g\, \delta_{i3} - I_i + \frac{\partial}{\partial x_j}(\phi\sigma^f_{ij}) = 0 \tag{A8}$$

where σ^f_{ij} is the stress within the fluid, and the sign of I_i is the reverse of that in (A7) because of Newton's third law. If (A7) and (A8) are to be useful they must be expressed in terms of the melt and

matrix velocities. The interphase volume force must obviously not depend on what frame is used to measure the velocities. Homsy *et al.* (1980) and Drew & Segel (1971) list a variety of functions of $\mathbf{v}$ and $\mathbf{V}$ which satisfy this condition. The simplest of these is simply the relative velocity of the melt with respect to the matrix, $\mathbf{v} - \mathbf{V}$. In addition Drew & Segel (1971) show that $\mathbf{I}$ must include a term due to the pressure in the fluid, to take account of the force which arises due to the gradient of ϕ. Hence the interphase force can be written as

$$\mathbf{I} = C_1(\mathbf{v} - \mathbf{V}) - P\nabla\phi \tag{A9}$$

where C_1 is a constant and P is the pressure in the melt. A variety of other terms could be included in (A9) but the resulting form of (A8) would no longer satisfy D'Arcy's law (see below).

The standard form for the stress tensor within an incompressible fluid is (Landau & Lifshitz, 1959)

$$\sigma_{ij} = -P\,\delta_{ij} + \mu\left(\frac{\partial v_i}{\partial x_j} + \frac{\partial v_j}{\partial x_i}\right) \tag{A10}$$

where μ is the dynamic viscosity. If the second term in (A10) is neglected, substitution of (A10) and (A9) into (A8) gives

$$\mathbf{v} - \mathbf{V} = -\frac{\phi}{C_1}\nabla(P + \rho_f g z) \tag{A11}$$

If $\mathbf{V} = 0$ (A11) corresponds to D'Arcy's law:

$$\phi\mathbf{v} = -\frac{k_\phi}{\mu}\nabla(P + \rho_f g z) \tag{A12}$$

where k_ϕ is the permeability, and μ is the viscosity of the melt. Hence (A11) and (A12) are the same if

$$C_1 = \mu\phi^2/k_\phi \tag{A13}$$

The stress within the matrix requires a more complicated expression than (A10). It is clear that, in the absence of gravity, a constant fluid pressure everywhere will not produce flow within the matrix, and hence

$$\sigma^s_{ij} = -P\,\delta_{ij} + \sigma'_{ij}(V) \tag{A14}$$

The porous matrix will compact if subject to an isostatic compression, and will expel fluid. It should therefore be regarded as a compressible fluid. If the rate of such compaction depends linearly on the applied stress it can be described by a bulk viscosity. The behaviour in shear is also likely to be linear if the stress is sufficiently small, and hence the stress σ'_{ij} can be written as (Landau & Lifshitz, 1959)

$$\sigma'_{ij} = \zeta^s\delta_{ij}\frac{\partial V_1}{\partial x_1} + \eta^s\left(\frac{\partial V_i}{\partial x_j} + \frac{\partial V_j}{\partial x_i} - \frac{2}{3}\delta_{ij}\frac{\partial V_1}{\partial x_1}\right) \tag{A15}$$

where ζ^s is the bulk viscosity and η^s the shear viscosity of the matrix and both may depend on ϕ. Equation (A15) is the simplest relation between σ'_{ij} and $\mathbf{V}$ which can describe the flow, and which will be valid at low stresses. The stresses involved in magma extraction are probably sufficiently small for (A15) to be justified. It is important to notice that σ'_{ij} in (A15) does not have zero trace. The definition of the pressure is therefore different from that usually adopted. If the pressure is defined as $-\frac{1}{3}\sigma^s_{ii}$ in this problem, it will contain a term which depends on the deformation rate. As Landau & Lifshitz (1959, p. 187) and Batchelor (1967, p. 154) point out, the thermodynamic pressure is defined only in equilibrium, and hence should not include terms dependent on the velocity gradient. It should also again be remarked that the equations governing the movement of the melt and matrix apply only to the mean motion on a scale large compared with that of the grains, and cannot for instance describe the deformation of an individual grain (Drew, 1983). On a scale comparable to that of a grain the matrix must be regarded as incompressible, and the appropriate solutions can be used to obtain an expression for the bulk viscosity (see Appendix C).

Substitution of (A9), (A13), (A14) and (A15) into (A7) leads to

$$-(1-\phi)\rho_s g\,\delta_{i3}+\frac{\mu\phi^2}{k_\phi}(v_i-V_i)-(1-\phi)\frac{\partial P}{\partial x_i}+\frac{\partial}{\partial x_j}(1-\phi)\,\sigma'_{ij}=0 \tag{A16}$$

where

$$(1-\phi)\sigma'_{ij}=\zeta\delta_{ij}\frac{\partial V_l}{\partial x_l}+\eta\left(\frac{\partial V_i}{\partial x_j}+\frac{\partial V_j}{\partial x_i}-\frac{2}{3}\delta_{ij}\frac{\partial V_l}{\partial x_l}\right) \tag{A17}$$

$$\zeta=(1-\phi)\,\zeta^x,\quad \eta=(1-\phi)\,\eta^x \tag{A18}$$

The term in (A16) involving k_ϕ can be eliminated using (A11), and, if ρ_f and ρ_s are constant and $D_V M/Dt=0$, the governing equations then become

$$\frac{\partial\phi}{\partial t}=-\nabla.\phi\mathbf{v}=\nabla.(1-\phi)\,\mathbf{V} \tag{A19}$$

$$\mathbf{v}-\mathbf{V}=-\frac{k_\phi}{\mu\phi}\nabla(P+\rho_f gz) \tag{A20}$$

$$-[(1-\phi)\rho_s+\phi\rho_f]\,g\,\delta_{i3}-\frac{\partial P}{\partial x_i}+\frac{\partial}{\partial x_j}[(1-\phi)\,\sigma'_{ij}]=0 \tag{A21}$$

Alternatively P can be eliminated from (A21) using (A20), and from (A20) by taking the curl of the equation, to give equations in terms of $\mathbf{v}$ and $\mathbf{V}$ only

$$\nabla\times\frac{\phi\mathbf{v}}{k_\phi}=\nabla\times\frac{\phi\mathbf{V}}{k_\phi} \tag{A22}$$

$$\frac{\partial}{\partial x_j}[(1-\phi)\,\sigma'_{ij}]=-\frac{\mu\phi}{k_\phi}(v_i-V_i)+(1-\phi)(\rho_s-\rho_f)g\,\delta_{i3} \tag{A23}$$

In a number of the examples discussed below ϕ is taken to be constant, when (A22) and (A23) can be written

$$\nabla\times\mathbf{v}=\nabla\times\mathbf{V} \tag{A24}$$

$$\left(\zeta+\frac{\eta}{3}\right)\nabla(\nabla.\mathbf{V})+\eta\nabla^2\mathbf{V}=-\frac{\mu\phi}{k_\phi}(\mathbf{v}-\mathbf{V})+(1-\phi)(\rho_s-\rho_f)g\mathbf{a}_z \tag{A25}$$

The governing equations and the stresses on the matrix are easily written out in cartesian coordinates. It is, however, helpful to use cylindrical and spherical coordinates for some problems. The expressions for ∇, $\nabla.$ and ∇^2 in cylindrical coordinates will be found in appendix 2 of Batchelor (1967). If the cylindrical axis is taken to be the z axis, with the radial coordinate being r, his x corresponds to z and his σ to r. The expressions for $\sigma'_{\theta z}$, σ'_{rz} and $\sigma'_{r\theta}$ are given on p. 51, equation (15.15) of Landau & Lifshitz (1959) and

$$\begin{aligned}
\sigma'_{rr}&=(\zeta^x-\tfrac{2}{3}\eta^x)\Delta+2\eta^x\frac{\partial V_r}{\partial r}\\
\sigma'_{\theta\theta}&=(\zeta^x-\tfrac{2}{3}\eta^x)\Delta+\frac{\eta^x}{r}\left(\frac{\partial V_\theta}{\partial\theta}+V_r\right)\\
\sigma'_{zz}&=(\zeta^x-\tfrac{2}{3}\eta^x)\Delta+2\eta^x\frac{\partial V_z}{\partial z}
\end{aligned} \tag{A26}$$

where $\Delta\equiv\nabla.\mathbf{V}$.

The corresponding expressions for $\sigma'_{r\theta}$, $\sigma'_{r\phi}$ and $\sigma'_{\theta\phi}$ in spherical coordinates are given on p. 52 of Landau & Lifshitz (1959) and

$$\sigma'_{rr} = (\zeta^x - \tfrac{2}{3}\eta^x)\Delta + 2\eta^x \frac{\partial V_r}{\partial r}$$

$$\sigma'_{\theta\theta} = (\zeta^x - \tfrac{2}{3}\eta^x)\Delta + 2\eta^x \left(\frac{1}{r}\frac{\partial V_\theta}{\partial \theta} + \frac{V_r}{r}\right) \tag{A27}$$

$$\sigma_{\phi\phi} = (\zeta^x - \tfrac{2}{3}\eta^x)\Delta + 2\eta^x \left(\frac{1}{r\sin\theta}\frac{\partial V_\phi}{\partial \phi} + \frac{V_r}{r} + \frac{V_\theta \cot\theta}{r}\right)$$

where $\Delta \equiv \nabla . \mathbf{V}$.

An important engineering application of these equations is to sintering and hot isostatic pressing, when the interaction and gravitational terms are absent. Equation (A23) then reduces to

$$\frac{\partial}{\partial x_j}[(1-\phi)\,\sigma'_{ij}] = 0 \tag{A28}$$

and if ϕ is constant (A24) and (A25) become

$$\nabla \times \mathbf{v} = \nabla \times \mathbf{V}$$

$$\left(\zeta + \frac{\eta}{3}\right)\nabla(\nabla . \mathbf{V}) + \eta\nabla^2\mathbf{V} = 0 \tag{A29}$$

Various simplifications can be made to (A25) by carrying out standard manipulations, and the resulting equations are then in convenient form for solution. The curl of (A25) is

$$\eta\nabla^2(\nabla \times \mathbf{V}) = -\frac{\mu\phi}{k_\phi}(\nabla \times \mathbf{v} - \nabla \times \mathbf{V}) \tag{A30}$$

(A24) shows that the right-hand side of this equation is zero, hence

$$\nabla^2(\nabla \times \mathbf{V}) = \nabla^2(\nabla \times \mathbf{v}) = 0 \tag{A31}$$

If the divergence of (A25) is taken, then

$$\left(\zeta + \frac{4\eta}{3}\right)\nabla^2(\nabla . \mathbf{V}) = -\frac{\mu\phi}{k_\phi}(\nabla . \mathbf{v} - \nabla . \mathbf{V}) \tag{A32}$$

Since ϕ is constant (A19) gives

$$\nabla . \mathbf{v} = -\frac{1-\phi}{\phi}\nabla . \mathbf{V}$$

and (A32) becomes

$$\nabla^2(\nabla . \mathbf{V}) - \frac{\mu}{k_\phi(\zeta + \frac{4}{3}\eta)}(\nabla . \mathbf{V}) = 0 \tag{A33}$$

If

$$x = \delta_c\, x', \quad y = \delta_c\, y', \quad z = \delta_c\, z'$$

where δ_c is a constant with the dimensions of length

$$\delta_c^2 = k_\phi \frac{(\zeta + \frac{4}{3}\eta)}{\mu} \tag{A34}$$

which will be referred to as the compaction length, (A33) becomes

$$\nabla'^2(\nabla' . \mathbf{V}) - (\nabla' . \mathbf{V}) = 0 \tag{A35}$$

where $\nabla' = \delta_c\, \nabla$.

The equations governing transport of heat and of a solute can also be obtained from the laws governing conservation of energy and mass respectively. There is, however, an interesting difference between these equations and those (A19) governing the behaviour of the melt and the matrix. Heat can diffuse between the melt and the matrix, and hence the heat content of each is not individually conserved. If the temperature variations are sufficiently slow, the melt and the matrix remain in thermal equilibrium. The conservation of energy then requires that the rate of change of energy within a volume should equal the rate at which heat is conducted across the surface S bounding V, the rate of heat generation within V, the rate at which the surface stresses do work on the matrix and the fluid, the rate of energy transport by the fluid motions and the work done by the body forces:

$$\frac{\mathrm{d}}{\mathrm{d}t}\int_V [\rho_s E_s(1-\phi) + \rho_f E_f \phi]\,\mathrm{d}V = -\int_S -k_T \nabla T.\,\mathbf{dS} + \int_V H\,\mathrm{d}V + \int_S \boldsymbol{\sigma}^s.\mathbf{V}(1-\phi).\,\mathbf{dS} + \int_S \boldsymbol{\sigma}^f.\mathbf{v}\phi\,\mathbf{dS}$$

$$-\int_S \rho_S E_S(1-\phi)\,\mathbf{V}.\,\mathbf{dS} - \int \rho_f E_f \phi\mathbf{v}.\,\mathbf{dS} + \int_V (1-\phi)\rho_S\,\mathbf{V}.\mathbf{g}\,\mathrm{d}V + \int_V \phi\rho_f\,\mathbf{v}.\mathbf{g}\,\mathrm{d}V \qquad \text{(A36)}$$

where E_f and E_S are the internal energies/unit mass of the melt and matrix respectively, k_T the thermal conductivity, H the rate of internal heat generation and $\mathbf{g}$ $(= -g\mathbf{a}_z)$ the vector gravitational acceleration. The kinetic energy is negligible and has been omitted. Use of (A3), (A4), (A7), (A9), (A13) and standard thermodynamic relationships leads to

$$T\Delta S\frac{\mathrm{D}_V M}{\mathrm{D}t} + (1-\phi)\rho_S T\frac{\mathrm{D}_V S_s}{\mathrm{D}t} + \phi\rho_f T\frac{\mathrm{D}_v S_f}{\mathrm{D}t} = \nabla.k_T\nabla T + \frac{\mu}{k_\phi}\phi^2(\mathbf{v}-\mathbf{V})^2$$

$$+ \zeta(\nabla.\mathbf{V})^2 + H + \frac{\eta}{2}\left(\frac{\partial V_i}{\partial x_j} + \frac{\partial V_j}{\partial x_i} - \frac{2}{3}\delta_{ij}\frac{\partial V_1}{\partial x_1}\right)^2 \equiv \Phi \qquad \text{(A37)}$$

ΔS is the change in entropy on converting from matrix to melt, $\mathrm{D}_V/\mathrm{D}t$ and $\mathrm{D}_v/\mathrm{D}t$ are the Lagrangian derivatives with respect to the matrix and the melt respectively, and S_s and S_f are the entropies/unit mass of the matrix and melt. The thermal conductivity of the mixture k_T should be obtained from the expression given by Budiansky (1970):

$$\frac{\phi}{2+\dfrac{k_T^f}{k_T}} + \frac{1-\phi}{2+\dfrac{k_T^s}{k_T}} = \tfrac{1}{3} \qquad \text{(A38)}$$

where k_T^s and k_T^f are the thermal conductivities of the matrix and melt respectively. (A37) can also be written in terms of the temperature

$$T\Delta S\frac{\mathrm{D}_V M}{\mathrm{D}t} + [(1-\phi)\rho_s C_p^s + \phi\rho_f C_p^f]\frac{\partial T}{\partial t} - T[(1-\phi)\alpha_s + \phi\alpha_f]\frac{\partial P}{\partial t} + (1-\phi)\rho_s C_p^s\mathbf{V}.\left[\nabla T - \frac{T\alpha_s\nabla P}{\rho_s C_p^s}\right]$$

$$+ \phi\rho_f C_p^f\,\mathbf{v}.\left[\nabla T - \frac{T\alpha_f\nabla P}{\rho_f C_p^f}\right] = \Phi \qquad \text{(A39)}$$

where C_p^s and C_p^f are the specific heats at constant pressure of the matrix and melt, α_s and α_f are the thermal expansion coefficients, and Φ is defined by (A37). The terms $T\alpha_s\nabla P/\rho_s C_p^s$ and $T\alpha_f\nabla P/\rho_s C_p^f$ are the adiabatic gradients of the matrix and melt respectively. It is useful to define the thermal diffusivity κ_T of the mixture as

$$\kappa_T = k_T/[(1-\phi)\rho_s C_p^s + \phi\rho_f C_p^f] \qquad \text{(A40)}$$

One further equation is required before this system of equations can be solved, which relates the amount of melt present, ϕ, to T and P. This relationship must be determined empirically, and a simple example of such a law is given in Appendix D.

The last conservation law which is needed is concerned with the concentration of a trace element or

isotope. This equation takes a simple form if the concentrations by weight in the melt c_f and the matrix c_s are in equilibrium and

$$c_s/c_f = K_c \tag{A41}$$

where K_c is the partition coefficient. Then

$$[(1-\phi)\rho_s K_c + \phi\rho_f]\frac{\partial c_f}{\partial t} + (1-\phi)\rho_s K_c \mathbf{V}\cdot\nabla c_f + \phi\rho_f \mathbf{v}.\nabla c_f = \rho_f \nabla.\phi\mathbf{D}^f\nabla c_f + (K_c - 1)\, c_f \frac{\mathrm{D}_v M}{\mathrm{D}t} \tag{A42}$$

where $\mathbf{D}^f$ is the diffusivity tensor of the solute in the melt. $\mathbf{D}^f$ can be strongly affected by the flow of the melt with respect to the matrix, and hence the diffusivity may be anisotropic. In partially melted rocks the diffusivity of the matrix is much smaller than that of the melt, and it has therefore been neglected in (A42). Generation of solute, by radioactive decay for instance, has also been neglected but can be included by adding an appropriate source term to the right hand side of (A42).

The equations derived in this appendix are all dimensional. The natural inclination of anyone with a geophysical fluid dynamics background is to rewrite all the equations, using δ_c as a length scale and τ_0 as a time scale, in dimensionless form, and in this way obtain the dimensionless constants which govern the form of the solutions. The temptation to proceed in this way has been resisted, principally because few people other than those with this background find the practice helpful. It will, however, be necessary to do so if the equations are to be solved numerically.

APPENDIX B

Initial compaction of a constant porosity layer onto an impermeable horizontal surface

A solution to the equations (A19) to (A21) is easily obtained when ϕ is initially constant and compaction of a half space occurs only in the vertical direction on to an impermeable surface on which both $\mathbf{v}$ and $\mathbf{V}$ are zero. Under these conditions

$$\mathbf{v} = (0, 0, w(z))$$
$$\mathbf{V} = (0, 0, W(z)) \tag{B1}$$

and (A33) becomes

$$\frac{\partial^3 W}{\partial z^3} - \frac{1}{\delta_c^2}\frac{\partial W}{\partial z} = 0 \tag{B2}$$

The solution to this equation which has $W = 0$ on $z = 0$

$$W = -w_0\,\phi(1 - \mathrm{e}^{-z/\delta_c}) \tag{B3}$$

where w_0 is a constant. The other solution involving e^{z/δ_c} must be excluded if W is to be finite for all z. (A19) requires

$$\frac{\partial w}{\partial z} = -\left(\frac{1-\phi}{\phi}\right)\frac{\partial W}{\partial z} \tag{B4}$$

hence the expression for w which satisfies the boundary conditions is

$$w = w_0(1-\phi)(1 - \mathrm{e}^{-z/\delta_c}) \tag{B5}$$

(A25) can be written as

$$(\zeta + \tfrac{4}{3}\eta)\frac{\partial^2 W}{\partial z^2} = -\frac{\mu\phi}{k_\phi}(w - W) + (1-\phi)(\rho_s - \rho_f)\, g \tag{B6}$$

and substitution of (B3) and (B5) into (B6) leads to an expression for w_0

$$w_0 = \frac{k_\phi}{\mu}\frac{(1-\phi)}{\phi}(\rho_s - \rho_f)\, g \tag{B7}$$

and the relative velocity of the melt with respect to the matrix is

$$w - W = w_0(1 - \mathrm{e}^{-z/\delta_c}) \tag{B8}$$

The last result which is needed is the initial rate of compaction of the matrix, given by (A19)

$$\frac{1}{\phi}\frac{\partial \phi}{\partial t} = -\frac{\partial w}{\partial z} = -\frac{w_0}{\delta_c}(1-\phi)\,e^{-z/\delta_c} \tag{B9}$$

The expression (B9) has the dimensions of reciprocal time, and defines a time scale τ for changes in porosity

$$\tau = \delta_c\, e^{z/\delta_c}/w_0(1-\phi) \tag{B10}$$

The solutions obtained above are valid only if ϕ is constant everywhere. Since (B9) shows that the rate of change of ϕ is not zero, the equations are strictly only valid at $t = 0$. In practice they will probably apply over time scales short compared with τ_0, where τ_0 is the minimum value of τ, at $z = 0$

$$\tau_0 = \delta_c/w_0(1-\phi) \tag{B11}$$

It is straightforward to extend these results to the problem of a compacting layer with $w = W = 0$ on two boundaries $z = 0$ and $z = h$. The other solution of (B3) must now be retained to give

$$W = -\frac{w_0\,\phi}{\sinh(h/\delta_c)}\left[\sinh\left(\frac{z-h}{\delta_c}\right) + \sinh\left(\frac{h}{\delta_c}\right) - \sinh\left(\frac{z}{\delta_c}\right)\right] \tag{B12}$$

$$w = -\left(\frac{1-\phi}{\phi}\right) W \tag{B13}$$

$$\frac{1}{\phi}\frac{\partial \phi}{\partial t} = \frac{(1-\phi)\,w_0}{\delta_c \sinh(h/\delta_c)}\left[\cosh\left(\frac{z}{\delta_c}\right) - \cosh\left(\frac{z-h}{\delta_c}\right)\right] \tag{B14}$$

Unlike (B9), (B14) is positive between $h/2$ and h (see Fig. 3). Hence the matrix expands throughout the upper half of the layer, and does so most rapidly at $z = h$. When ϕ reaches a critical value, which is estimated in section 3 to be about 0·2, the matrix will disaggregate. This will first happen on $z = h$. Thereafter a layer of melt will accumulate and the upper surface of the matrix will be free. If the stress in the vertical direction is to vanish (A15) shows that

$$\frac{\partial W}{\partial z} = 0 \tag{B15}$$

Solution of (B2), (B4) and (B6) then gives

$$W = -w_0\,\phi\left[1 - \frac{\cosh\left(\dfrac{h-z}{\delta_c}\right)}{\cosh\left(\dfrac{h}{\delta_c}\right)}\right] \tag{B16}$$

$$w = -\left(\frac{1-\phi}{\phi}\right) W \tag{B17}$$

$$\frac{1}{\phi}\frac{\partial \phi}{\partial t} = -\frac{w_0}{\delta_c}(1-\phi)\frac{\sinh\left(\dfrac{h-z}{\delta_c}\right)}{\cosh\left(\dfrac{h}{\delta_c}\right)} \tag{B18}$$

where the layer extends from $z = 0$ to h, and w_0 is given by (B7). Since $\sinh(h-z)/\delta_c$ is positive throughout this range, $\partial\phi/\partial t < 0$ everywhere.

Equations (B16) to (B18) are useful because they describe the behaviour in two limits, $h/\delta_c \gg 1$ and $h/\delta_c \ll 1$. In the first case

$$\frac{\cosh\left(\frac{h-z}{\delta_c}\right)}{\cosh\left(\frac{h}{\delta_c}\right)} \to e^{-z/\delta_c} \tag{B19}$$

$$\frac{\sinh\left(\frac{h-z}{\delta_c}\right)}{\cosh\left(\frac{h}{\delta_c}\right)} \to e^{-z/\delta_c} \tag{B20}$$

and (B16) to (B18) reduce to (B3), (B5) and (B9). This result is not surprising, since the upper boundary of the layer is in a region where the half space solution shows that compaction is not occurring. Hence $\partial W/\partial z = 0$ throughout this region, and the introduction of a free boundary does not affect the half space solution.

A more interesting limit is $h/\delta_c \ll 1$, when

$$W = -\frac{w_0 \phi}{2\delta_c^2} z(2h - z) \tag{B21}$$

$$w = -\left(\frac{1-\phi}{\phi}\right) W \tag{B22}$$

$$\frac{1}{\phi}\frac{\partial \phi}{\partial t} = -\frac{w_0}{\delta_c^2}(1-\phi)(h-z) \tag{B23}$$

The factor w_0/δ_c^2 occurs in all these expressions, multiplied by some function of ϕ, h and z. Substitution of (A34) and (B7) gives

$$\frac{w_0}{\delta_c^2} = \frac{1-\phi}{\phi}\frac{(\rho_s - \rho_f)g}{\zeta + \frac{4}{3}\eta} \tag{B24}$$

Thus w_0/δ_c^2 is independent of the viscosity μ of the melt, and of the permeability k_ϕ of the matrix.

The velocities can be made dimensionless by using w_0 as a velocity scale and δ_c as a length scale

$$z' = z/\delta_c, \quad W' = W/w_0, \quad w' = w/w_0 \tag{B25}$$

$$t' = t w_0/\delta_c \tag{B26}$$

The velocities and compaction rates scaled in this way for $h' = 4$ are plotted in Fig. 1 ((B16) to (B18)) and Fig. 3 ((B12) to (B14)). These figures also show the dissipation in the matrix and the melt, obtained from (A37). That in the matrix is

$$\zeta(\nabla . \mathbf{V})^2 + \frac{\eta}{2}\left(\frac{\partial V_i}{\partial x_j} + \frac{\partial V_j}{\partial x_i} - \frac{2}{3}\delta_{ij}\frac{\partial V_l}{\partial x_l}\right)^2 = \frac{\mu w_0^2}{k_\phi}\left(\frac{\partial W'}{\partial z'}\right)^2 \tag{B27}$$

and in the melt is

$$\frac{\mu}{k_\phi}\phi^2(\mathbf{v} - \mathbf{V})^2 = \frac{\mu w_0^2}{k_\phi} W'^2 \tag{B28}$$

Only $(\partial W'/\partial z')^2$ and W'^2 are plotted. The solution for the thin layer approximation with $h' = 0{\cdot}5$ is shown in Fig. 2 ((B21) to (B23)).

APPENDIX C

Some special solutions

Pharr & Ashby (1983) compressed a cylinder of porous material by loading its ends, and measured the rate of shortening. The permeability of the cylinders of KCl which they used was sufficiently large for the flow to be controlled by the deformation of the matrix alone, and hence by (A29). If the z component of the velocity is W then

$$W = -Az \tag{C1}$$

where A is the strain rate in z direction and is assumed to be positive. Writing (A29) in cylindrical polar coordinates, and assuming V_r to be a function of r only, gives

$$\left(\zeta + \frac{4\eta}{3}\right)\frac{\mathrm{d}}{\mathrm{d}r}\frac{1}{r}\left[\frac{\mathrm{d}}{\mathrm{d}r}(rV_r)\right] = 0. \tag{C2}$$

The solution to (C2) which is finite at $r = 0$ is

$$V_r = Cr \tag{C3}$$

where C is a constant. In some of Pharr and Ashby's experiments $\sigma_{rr} = 0$, a condition which requires

$$C = \frac{A}{2}\frac{(\zeta - \frac{2}{3}\eta)}{\zeta + \eta/3} \tag{C4}$$

Then the normal stress on the end of the cylinder σ_{zz} is given by

$$\sigma_{zz} = -\frac{3\eta\zeta}{\zeta + \eta/3}A \tag{C5}$$

Pharr & Ashby (1983) measured σ_{zz} and A. To determine both η and ζ it is necessary also to measure the radial strain rate C.

It is more satisfactory to determine ζ and η independently. The radial compaction of a spherical body must satisfy (A29) in spherical polar coordinates. If both other components of V are zero V_r must satisfy

$$\frac{\mathrm{d}}{\mathrm{d}r}\left[\frac{1}{r^2}\frac{\mathrm{d}}{\mathrm{d}r}(r^2V_r)\right] = 0 \tag{C6}$$

Hence

$$V_r = \frac{Cr}{3} \tag{C7}$$

where C is a constant. The other solution is singular at the origin. The radial stress σ_{rr} is given by

$$\begin{aligned}\sigma_{rr} &= C\zeta \\ &= 3\zeta\left(\frac{V_r}{r}\right)\end{aligned} \tag{C8}$$

Therefore the bulk viscosity can be determined from the radial strain rate V_r/r when the sphere is subjected to a known normal stress.

Alternatively the densification rate can be measured when the body is subjected to a constant pressure P on its external surface. Such an experiment could be carried out by enclosing the body in a thin rubber membrane. Then from (A19) the densification rate

$$\frac{\partial\phi}{\partial t} = (1-\phi)\,\nabla.\mathbf{V} = (1-\phi)\,C \tag{C9}$$

(C8) then gives

$$C = -\frac{P}{\zeta} \tag{C10}$$

and

$$\zeta = \frac{(1-\phi)P}{\left(-\frac{\partial \phi}{\partial t}\right)} \tag{C11}$$

Artz *et al.* (1982) write $-\partial\phi/\partial t$ as $\dot{D}$ and P as p_2^x. Their expression (20) is identical to (C11) if

$$\zeta = (1-\phi)\frac{[3(\phi^{2/3}-1)+(1+\phi^{2/3})\log_e 1/\phi]}{1-\phi^{2/3}}\frac{kTa^3}{54\Omega D_b \delta} \tag{C12}$$

where k is Boltzmann's constant, Ω is the atomic volume and $D_b\delta$ is the grain boundary thickness multiplied by the grain boundary diffusion coefficient, and lattice diffusion has been neglected.

APPENDIX D

Melting produced by the reduction of pressure at constant entropy

The mathematical description of melting when the melt and matrix move independently requires the equations governing the conservation of mass, momentum and energy of a two phase flow (A3), (A4), (A20), (A21), and (A39) to be solved, taking account of the transformation of matrix into melt, and is not attempted here. The complications are less if the melt and matrix move with the same velocity, and the equations become analytically tractable if the melting process takes place at constant entropy.

The simplest case to consider is the melting of a monominerallic rock, but it has the disadvantage that the temperature is a function only of depth if melt is present. It is useful to be able to discuss the influence of melting on the geotherm, and to do so the model must include more than one component in the rock. If the entropy S is to be constant (Verhoogen, 1965)

$$\mathrm{d}S = \left(\frac{\partial S}{\partial X}\right)_{P,T}\mathrm{d}X + \left(\frac{\partial S}{\partial T}\right)_{X,P}\mathrm{d}T + \left(\frac{\partial S}{\partial P}\right)_{X,T}\mathrm{d}P = 0 \tag{D1}$$

where X is the melt fraction by weight. X is related to the volume fraction of melt ϕ through

$$\phi = \frac{X\rho_s}{\rho_f + X(\rho_s - \rho_f)} \tag{D2}$$

Maxwell's relationships and other standard thermodynamic identities can be used to convert (D1) to

$$\Delta S\,\mathrm{d}X + [(1-X)C_p^s + XC_p^f]\frac{\mathrm{d}T}{T} - \left[\frac{\alpha_s}{\rho_s} + \left(\frac{\alpha_f}{\rho_f} - \frac{\alpha_s}{\rho_s}\right)X\right]\mathrm{d}P = 0 \tag{D3}$$

where ΔS is the change in entropy on changing from solid to melt, C_p is the specific heat at constant pressure and α the thermal expansion coefficient. (D3) can also be obtained from (A37) if the right hand side is zero and $\mathbf{v} = \mathbf{V}$, since

$$\mathrm{d}M = [(1-\phi)\rho_s + \phi\rho_f]\,\mathrm{d}X \tag{D4}$$

and

$$X = \frac{\phi\rho_f}{(1-\phi)\rho_s + \phi\rho_f} \tag{D5}$$

(D3) can only be integrated if the variation of T with X and P is known:

$$T = T(X,P) \tag{D6}$$

Then if $C_p^f = C_p^s$, (D3) becomes

$$\frac{\mathrm{d}X}{\mathrm{d}P} = \frac{-\frac{C_p}{T}\left(\frac{\partial T}{\partial P}\right)_x + \frac{\alpha_s}{\rho_s} + \left(\frac{\alpha_f}{\rho_f} - \frac{\alpha_s}{\rho_s}\right)X}{\Delta S + \frac{C_p}{T}\left(\frac{\partial T}{\partial X}\right)_p} \tag{D7}$$

(D7) was integrated numerically, using a fourth order Runge–Kutta scheme and starting on the solidus ($X = 0$) at a given temperature. At each X, P the temperature was obtained from (D6). The relationship between T, X and P must be obtained from laboratory measurements.

A simple form for (D6) is

$$(T - 273) = 1100 + 100P + 600X \tag{D8}$$

where P is in GPa. Fig. 7*a* and *b* show $X(T)$ and $P(T)$ obtained by integrating (D7) and (D8). It is also of interest to obtain the total thickness of melt $t_f(z)$ (Fig. 7*c*) below a level z by integration

$$t_f(z) = \int_{z_0}^{z} \phi(z)\, dz \tag{D9}$$

where z_0 is the position of the solidus. Since (D9) is only accurate if the melt and matrix do not move with respect to each other, $t_f(z)$ does not accurately determine the quantity of melt which can be extracted from below z. An accurate determination will require the solution of the equations in Appendix A, similar to that carried out by Ahern and Turcotte, but taking proper account of the deformation of the matrix. Such a calculation still depends on the form of (D6) and the value assumed for ΔS. Neither are accurately known, and it therefore seemed worthwhile to investigate whether the error which results from using (D9) to estimate the volume of magma which can be extracted is larger than the probable uncertainty in (D6) and ΔS. The two principal effects of the movement of magma are heat transport by the melt and release of gravitational potential energy. If all the heat produced by both effects is absorbed by increasing the melt fraction, an upper bound on $t_f(z)$ can be obtained. Magma rising from a position z to the surface z_1 isentropically, will have a temperature θ at z_1 of approximately

$$\theta = T(z) - \frac{\alpha_f g T(z_1)}{C_p}(z_1 - z) \tag{D10}$$

Since $\theta > T(z_1)$ the melt can increase its volume at z_1 by melting the matrix. A unit mass of melt can increase to no more than $1 + \Delta m$ where

$$\Delta m = \frac{C_p(\theta - T(z_1))}{T(z_1)\Delta S} \tag{D11}$$

The force exerted on a unit volume of magma during its ascent is

$$(\rho_s - \rho_f)g \tag{D12}$$

and therefore the work done is no greater than

$$\left(\frac{\rho_s}{\rho_f} - 1\right) P(z) \tag{D13}$$

If all this work is converted into melt, the volume ΔV generated is

$$\Delta V = \frac{P(z)\left(\frac{\rho_s}{\rho_f} - 1\right)}{\rho_f T(z_1)\Delta S} \tag{D14}$$

The effect of including both these terms is to increase $t_f(z_1)$ by up to 60 per cent in the most extreme case (Fig. 8). The effect of retraining 3 per cent of the melt in the matrix is therefore negligible.

The calculations were carried out for two other expressions for $T(X, P)$

$$T = T_s + \left(\frac{\partial T}{\partial X}\right)_p X$$

$$(T_s - 273) = 1100 + \frac{650}{\pi}\tan^{-1}[1{\cdot}8(P - 1{\cdot}75)] \tag{D15}$$

$$\left(\frac{\partial T}{\partial X}\right)_p = 362 - \frac{534}{\pi}\tan^{-1}[3{\cdot}66(P - 1{\cdot}75)]$$

where P is in GPa. (D15) is empirical, and the form was chosen to fit the observations of Mysen & Kushiro (1977) and Jaques & Green (1980) (Fig. 10) as well as possible. Another, somewhat simpler, expression was also used:

$$\begin{aligned}(T-273) &= 1115 + 120P + (600 - 136P)X, \quad P < 3{\cdot}5 \text{ GPa} \\ &= 1115 + 120P + 124X, \quad P > 3{\cdot}5 \text{ GPa}\end{aligned} \tag{D16}$$

APPENDIX E

Diffusion and dispersion

In the derivation of (A39) the temperatures of the melt and matrix were assumed to be the same. A similar assumption of equilibrium between melt and matrix was made in deriving (A42). It is important to investigate the conditions which must be satisfied if these assumptions are to be valid. A straightforward method of doing so is to determine the time scales for the various changes involved. The time required for a single grain to reach thermal equilibrium, τ_{gr}, is

$$\tau_{gr} \sim a^2/\kappa_T. \tag{E1}$$

Changes in temperature can be produced by either conduction or advection of heat. (A39) shows that the conductive time scale τ_{cond} is

$$\tau_{cond} \sim l^2/\kappa_T \tag{E2}$$

where l is the length scale over which the temperature varies. Similarly the advection time scale τ_{adv} is

$$\tau_{adv} \sim l/\phi|\mathbf{v}| \tag{E3}$$

where $|\mathbf{v}|$ is the magnitude of the velocity of the melt. For the purposes of all these estimates the differences in thermal properties between the matrix and the melt can be ignored. If (A39) is to describe the temperature both τ_{cond} and τ_{adv} must be much greater than τ_{gr}. The first condition requires

$$l \gg 1 \text{ mm} \tag{E4}$$

which is easily satisfied. The condition that

$$\tau_{adv} \gg \tau_{gr} \tag{E5}$$

requires

$$\frac{l\kappa_T}{\phi a^2} \gg |\mathbf{v}|. \tag{E6}$$

Substitution of the values in Table 1 gives

$$10l \gg |\mathbf{v}| \tag{E7}$$

where $|\mathbf{v}|$ is in metres/second. Since the velocities in partial melts will not exceed a metre/year, (E7) is always satisfied. Hence the assumptions leading to (A39) are justified.

Similar arguments can be used to examine the validity of (A42). However, unlike the diffusibility of heat, the volume diffusivity of the matrix D_s is very different from that of the melt D_f. Hence

$$\tau_{gr} \sim a^2/D_s \tag{E8}$$

and

$$\tau_{cond} \sim l^2/D_f \tag{E9}$$

hence

$$\tau_{cond} \gg \tau_{gr}$$

if

$$l \gg \left(\frac{D_f}{D_s}\right)^{1/2} a \simeq 3 \text{ m} \tag{E10}$$

The other condition is somewhat more restrictive. (A42) shows that

$$\tau_{adv} \sim \left[\left(\frac{1}{\phi} - 1\right) K_c + 1\right] \frac{l}{|\mathbf{v}|}. \tag{E11}$$

Many elements of interest are concentrated in the melt, and hence the term in square brackets in (E11) is ~ 1. Therefore, if

$$\tau_{adv} \gg \tau_{gr} \tag{E12}$$

$$\frac{lD_s}{a^2} \gg |\mathbf{v}|. \tag{E13}$$

Substitution then gives

$$3 \times 10^{-4}\, l \gg |\mathbf{v}| \tag{E14}$$

where $|\mathbf{v}|$ is measured in metres/year. If the upper bound of $|\mathbf{v}|$ is 1 m yr^{-1} (A42) will only be valid for concentration variations whose size exceeds 300 m. Of all the four conditions, (E14) is the one most likely to be violated.

A useful solution to (A42) can now be obtained in a reference frame fixed to the matrix if ϕ and $\mathbf{v}$ are constant everywhere, and if $\mathbf{v}$ can be written

$$\mathbf{v} = (0, 0, w) \tag{E15}$$

If the concentration c_f is a function only of z then (A42) becomes

$$\left[\frac{(1-\phi)}{\phi}\frac{\rho_s}{\rho_f} K_c + 1\right] \frac{\partial c_f}{\partial t} + w \frac{\partial c_f}{\partial z} = D_{33} \frac{\partial^2 c_f}{\partial z^2} \tag{E16}$$

where D_{33} is the appropriate element of the diffusivity tensor $\mathbf{D}_f$, which is assumed to have a principal axis in the z direction (see Dullien, 1979, Ch. 7). Equation (E16) can be written as

$$\frac{\partial c_f}{\partial t} + w_e \frac{\partial c_f}{\partial z} = D_e \frac{\partial^2 c_f}{\partial z^2} \tag{E17}$$

where

$$w_e = Fw \tag{E18}$$

$$D_e = FD_{33} \tag{E19}$$

and

$$F = \left[\left(\frac{1-\phi}{\phi}\right)\frac{\rho_s}{\rho_f} K_c + 1\right]^{-1} \tag{E20}$$

A solution to (E17) is

$$c_f(z,t) = \frac{c_0}{\sqrt{4D_e t}} \exp\left[-\frac{(z - w_e t)^2}{4D_e t}\right] \tag{E21}$$

where c_0 is a constant.

Equation (E21) represents a gaussian variation of concentration, whose peak is at $z - w_e t$. In this form the solution is not very useful, because $c_f(0,t) \to \infty$ as $t \to 0$. If, however, the origin is moved in space and time using

$$\begin{aligned} z &= z' + z_1 \\ t &= t' + t_1 \end{aligned} \tag{E22}$$

where

$$\begin{aligned} z_1 &= w_e h^2/4D_e \\ t_1 &= h^2/4D_e \end{aligned} \tag{E23}$$

and h is a constant, (E21) becomes

$$c_f(z',t') = \frac{1}{\sqrt{1 + t'/t_1}} \exp\left[-\frac{(z' - w_e t')^2}{4D_e(t' + t_1)}\right] \tag{E24}$$

and represents a gaussian function whose amplitude is unity when $z' = t' = 0$, and 1/e when $z' = h$, $t' = 0$. (E24) was used to obtain Figs. 16 and 17, with $D_{33} = D_f$. (E21) and (E24) show that the concentration peak does not move with the velocity of the melt, but with a reduced velocity w_e. The factor F by which the velocity is reduced depends on the distribution between the melt and the matrix. The partially melted region therefore behaves in a similar way to a standard separation column, and different elements will move through the matrix with different velocities. The diffusion coefficient is also reduced by the presence of the matrix.

The solution for $c_f(z,t)$ given by (E21) can also be used to investigate dispersion when it is produced by the geometry of the flow itself, rather than by diffusion. The condition which must be satisfied if this regime is to apply is that the time taken for the solute to diffuse a distance a in the liquid must be long compared with the time taken for the liquid to be advected the same distance. Equations (E8) and (E11) then show that this condition requires

$$\frac{a|v|}{FD_f} \gg 1 \tag{E25}$$

When (E25) is satisfied, the longitudinal diffusion coefficient D_{33} can be written as (see Dullien 1979, Fig. 7.12).

$$D_{33} = C_{33}\, w \tag{E26}$$

where C_{33} is a constant. The transverse diffusion coefficients are equal if the material is isotropic, and can be written in the same way. The value of C_{11} is, however, smaller than C_{33}. Substitution of (E26) into (E21) then gives

$$c_f(z,z_1) = \frac{c_0}{\sqrt{4C_e z_0}} \exp\left[-\frac{(z - z_0)^2}{4C_e z_0}\right] \tag{E27}$$

where

$$C_e = FC_{33} \tag{E28}$$

$$z_0 = w_e t \tag{E29}$$

The form of (E27) is somewhat surprising, since it shows that c_f depends only on z_0, the distance travelled at the effective velocity w_e, and not on w_e itself. Hence if (E25) is satisfied the dispersion will depend only on the thickness of the compacting layer, and not on the rate at which compaction occurs.

Many materials of geological interest contain several solid phases. The expressions (E21)–(E29) also apply to such materials if F is defined by

$$F = \left[\frac{\sum_{i=1}^{n} f_i \rho_i K_{ci}}{\phi \rho_f} + 1\right]^{-1} \tag{E30}$$

where f_i is the volume fraction occupied by the solid phase i, whose distribution coefficient is K_{ci} and density ρ_i. The summation must be taken over all n solid phases.